ASSESSMENT OF THE EFFECTS OF PLASMA BUBBLES ON GAIM-GM

THESIS

Kenneth R. Fenton Jr., Captain, USAF

AFIT/GAP/ENP/11-S02

DEPARTMENT OF THE AIR FORCE
AIR UNIVERSITY

AIR FORCE INSTITUTE OF TECHNOLOGY

Wright-Patterson Air Force Base, Ohio

AFIT/GAP/ENP/11-S02

ASSESSMENT OF THE EFFECTS OF PLASMA BUBBLES ON GAIM-GM

THESIS

Presented to the Faculty

Department of Engineering Physics

Graduate School of Engineering and Management

Air Force Institute of Technology

Air University

Air Education and Training Command

In Partial Fulfillment of the Requirements for the

Degree of Master of Science

Kenneth R. Fenton Jr., BS

Captain, USAF

September 2011

AFIT/GAP/ENP/11-S02

ASSESSMENT OF THE EFFECTS OF PLASMA BUBBLES ON GAIM-GM

Kenneth R. Fenton Jr., BS

Captain, USAF

Approved:

_____	_____
William F. Bailey, PhD (Chairman)	Date
_____	_____
Lt Col Ariel O. Acebal (Member)	Date
_____	_____
Ludger Scherliess, PhD (Member)	Date

Abstract

Plasma bubbles are regions of depleted plasma density generated in the post-sunset equatorial region of the ionosphere. Bubbles significantly affect total electron count (TEC) and consequently alter communication and navigation capabilities. Here, the Global Assimilation of Ionospheric Measurements Gauss-Markov (GAIM-GM) model is studied in order to assess its capability to accurately model equatorial plasma bubbles. GAIM-GM uses the Ionospheric Forecast Model (IFM) as a background state modified through the application of a Kalman Filter to incorporate ionospheric observations such as Global Positioning System (GPS) total electron content (TEC) values. GPS TEC values representative of plasma bubble conditions are modeled and input into GAIM-GM along with a background IFM state and compared with GAIM-GM model runs with plasma bubbles absent. The model resolution, bubble depletion factor, filter time constant, and geophysical conditions are varied to assess model response. GAIM-GM is unable to reliably model plasma bubble magnitude and spatial extent due to several characteristics of the model and filter. The resolution of GAIM-GM, in both regional and global modes, is insufficient to capture the small scale of bubbles. Additionally, the sun synchronous movement of perturbations and lower bound of the Kalman filter affect the location and magnitude of depletion regions in the model.

Acknowledgments

I would like to express my sincere appreciation to my faculty advisor, Dr. William Bailey, for his guidance and support throughout the course of this thesis effort. He was always there to point me in the right direction while still allowing me a large measure of independence in the research process. It was a pleasure to work with a professor of such great knowledge and wit.

I would also like to thank the rest of my thesis committee. Lt Col Acebal always kept an operational focus and shed light upon the importance of the research at hand. His ideas and dedication proved invaluable to my work. Dr. Scherliess from Utah State University was able to ease my process by making the distance seem not quite so far. He was always quick to respond to my questions and his answers and extra work aided me immensely.

I would also like to thank the rest of the staff at Utah State University, Drs. Robert Schunk and Li Zhu for their interest and involvement, with a special thanks to Dr. Larry Gardner who responded quickly to our every request despite his own large workload. Finally, Dr. Don Thompson set the tone for this project early on and was able to teach me how to run the models from afar. His work was instrumental in getting this research to the level it needed to be.

Kenneth R. Fenton Jr.

Table of Contents

Page

List of Figures

List of Tables

ASSESSMENT OF THE EFFECTS OF PLASMA BUBBLES ON GAIM-GM

I. Introduction

1.1 Background

Plasma bubbles are regions of severely depleted plasma densities commonly found in the Earth's equatorial ionosphere. The sharp density gradients associated with plasma bubbles can cause disruption of radio and satellite communication. HF radio communication and GPS are examples of two systems the military has grown dependent on that are affected by the ionosphere. The presence of plasma bubbles can lead to radio blackouts and GPS signal outages that are detrimental to both civilian and military operations.

The Global Assimilation of Ionospheric Measurements Gauss Markov (GAIM-GM) model is a leading ionospheric representation that is used by the Air Force. Specifications and forecasts created by GAIM-GM are used by the Air Force in space and air operations. The accuracy of the model affects operational and tactical military planning. Commanders and mission planners need to know the reliability and tolerances of decision aids to effectively utilize resources.

1.2 Problem Statement

Like terrestrial weather models, it is important to understand the capabilities and limitations of an ionospheric model. Operationally, it is necessary for mission planners and forecasters to understand the capability of GAIM-GM to include plasma bubbles in its output. Computationally, exploring the limits of current systems forges the road ahead for improvements to predictive capabilities.

1.3 Research Objective

The research objective is to determine the capability of GAIM-GM to model plasma bubbles. GAIM-GM does not include the necessary physics to allow for the consistent reconstruction of plasma bubble structures. Plasma bubbles will be imposed upon the input of GAIM-GM and the effects of the bubbles upon the output studied. The results will be useful to both space weather forecasters and future model developers. Model developers will be able to incorporate the results into future ionospheric models to better handle plasma bubbles. Space weather forecasters will better understand the capabilities of the present model and be able to tailor their products accordingly.

1.4 Preview

The following chapters will chronicle the research conducted to determine the capability of GAIM-GM to model plasma bubbles. Chapter 2 will provide background information on plasma bubbles, GAIM-GM, and GPS ionospheric measurements. Next, Chapter 3 will cover the methodology used to conduct the research, including the placement of plasma bubble observations within GAIM-GM and the model parameters

adjusted in the study. Then results of the tests involving various model parameters will be presented in Chapter 4. Finally, Chapter 5 will conclude with an assessment of GAIM-GM's performance, recommendations, and suggestions for future study.

II. Literature Review

This chapter will provide background information on topics relevant to research on the capability of GAIM-GM to model equatorial plasma bubbles. First, the Earth's ionosphere will be discussed because plasma bubbles occur in this layer of the atmosphere. Next, a section describing plasma bubbles will be presented, to include the formation process and characteristics. A discussion on calculating Total Electron Content (TEC) from the GPS network will follow. Finally, GAIM-GM will be described, including discussions on the Ionospheric Forecast Model (IFM) and the Kalman filter.

2.1 Ionosphere

The ionosphere is the region of the atmosphere where significant numbers of free thermal electrons and ions are present. Solar extreme ultraviolet (EUV) radiation and particle precipitation are two significant sources of energy input into the ionosphere. Within the EUV spectrum relatively longer wavelengths cause dissociation while shorter wavelengths cause ionization. The sinks of ionospheric energy are airglow and neutral heating of the thermosphere. The ion density is controlled by the balance of photoionization production, ion transport, and recombination losses. The ionosphere is located from 60 km above the surface of the Earth to altitudes greater than 1000 km. The ionosphere is generally divided into four regions, the D, E, F1, and F2 layers, as shown in Figure 1. The F2 layer has the greatest ion density and consequently impact on radio and satellite signal propagation. At equatorial latitudes the plasma density of the ionosphere is higher during the day due to solar photoionization, while at night solar photoionization ends and recombination significantly decreases the plasma densities of the D and E

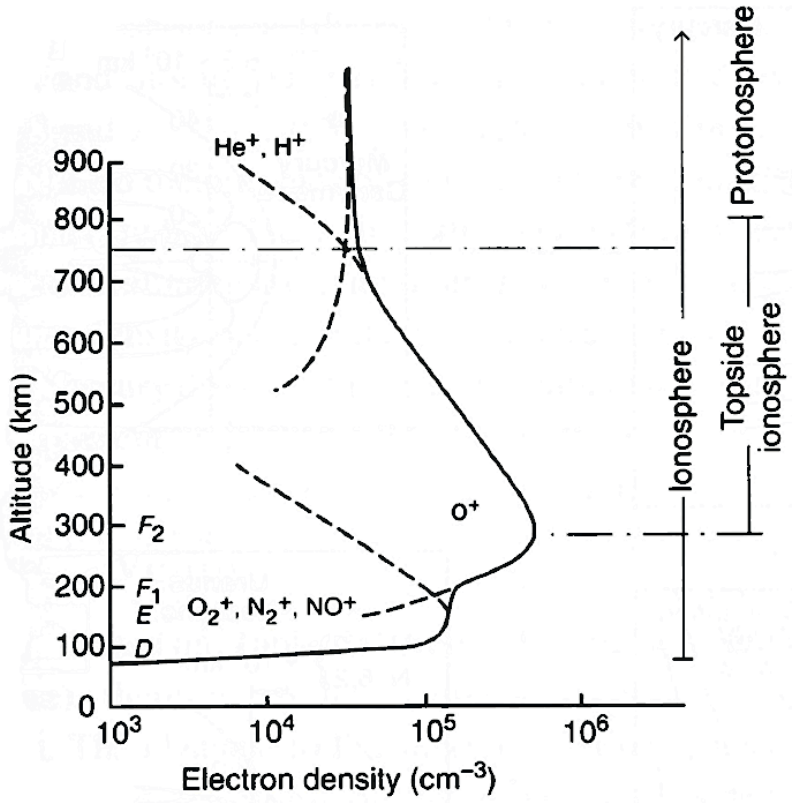

Figure 1. The layers of the Earth's daytime ionosphere. From Schunk and Nagy, 2009.

layers. Plasma densities in the ionosphere vary with season, time of day, solar cycle, and geomagnetic activity. Irregularities in the plasma density are known to occur and some of the most severe ones are called plasma bubbles (Schunk and Nagy, 2009).

2.2 Plasma Bubbles

Plasma bubbles are regions of reduced F region plasma densities that form along the bottomside F region (200 km) and extend vertically into the topside ionosphere. Also known as plasma depletions or holes, plasma bubbles have characteristic spatial and temporal patterns that have been studied for more than 30 years (Sinha and Raizada, 2000). The bubbles increase ionospheric scintillations resulting in disruption or

degradation of transionospheric communications and navigation systems (Sahai et al, 2000).

Plasma bubbles were first observed as "ion density biteouts" by Hanson and Sanatai in 1973 using in situ satellite probes. The bubbles manifest themselves as regions of low intensity in night airglow images. Modern methods of detecting these ionospheric anomalies include ionosondes, incoherent scatter radars, in situ rockets and satellites, and wide angle airglow imaging systems (Sinha and Raizada, 2000). Currently, GPS offers continuous monitoring of the generation and evolution of plasma bubbles on a large scale, due to its permanent operation and near global coverage (Portillo et al, 2008).

2.2.1 Development

Plasma bubbles begin as Rayleigh-Taylor instabilities in the bottomside of the equatorial F layer (Burke et al, 2004). The bubbles form as density perturbations which are believed to be caused by gravity waves. The resulting instability propagates upwards through the post sunset F region (Li et al, 2009).

Plasma bubbles are the result of dynamo electric fields, which are generally eastward during the day and westward at night. During the day the eastward electric field produces an upward $\vec{E}$x$\vec{B}$ drift of the F region plasma. Near dusk the eastward electric field is enhanced, referred to as the prereversal enhancement, before it turns westward. The F region consequently rises due to the stronger upward $\vec{E}$x$\vec{B}$ drift as the ionosphere corotates into the darkness. In the darkness the lower part of the F region is further depleted by recombination where the ion-neutral collision frequency is high. The result

is a raised F region with a steep vertical, bottomside density gradient (Schunk and Demars, 2003).

The steep density gradient, shown at the top of Figure 2, is supported by the strong magnetic field. Initially no electric fields are present but when a perturbation occurs, charge build up leads to electric fields in the $\hat{y}$ component. Electric fields in the positive $\hat{y}$ direction lead to an upwards $\vec{E}$x$\vec{B}$ drift that allows the instability to grow into small density irregularities, or spread F. During severe spread F, plasma bubbles form on the bottomside F layer and drift upwards with speeds that generally vary from 100 to 500 m/s (Schunk and Nagy, 2009).

As the instability moves upwards the entire north-south extent of the magnetic flux tube becomes depleted. The bubble takes the form of a vertically elongated wedge of depleted plasma, resembling an upside down watermelon slice, that can be hundreds of kilometers wide (Schunk and Demars, 2003).

2.2.2 Characteristics

Plasma bubbles are most likely to form in regions where the ends of magnetic flux tubes encounter the dusk terminator simultaneously. At longitudes where the magnetic declination is zero, plasma bubble formation is favored near the equinoxes. In regions of westward (eastward) magnetic declination, the minimum angle between the flux tubes and the dusk terminator shifts towards the December (June) solstice. Most plasma bubbles are observed within 15 degrees of the geomagnetic equator (Burke et al, 2004).

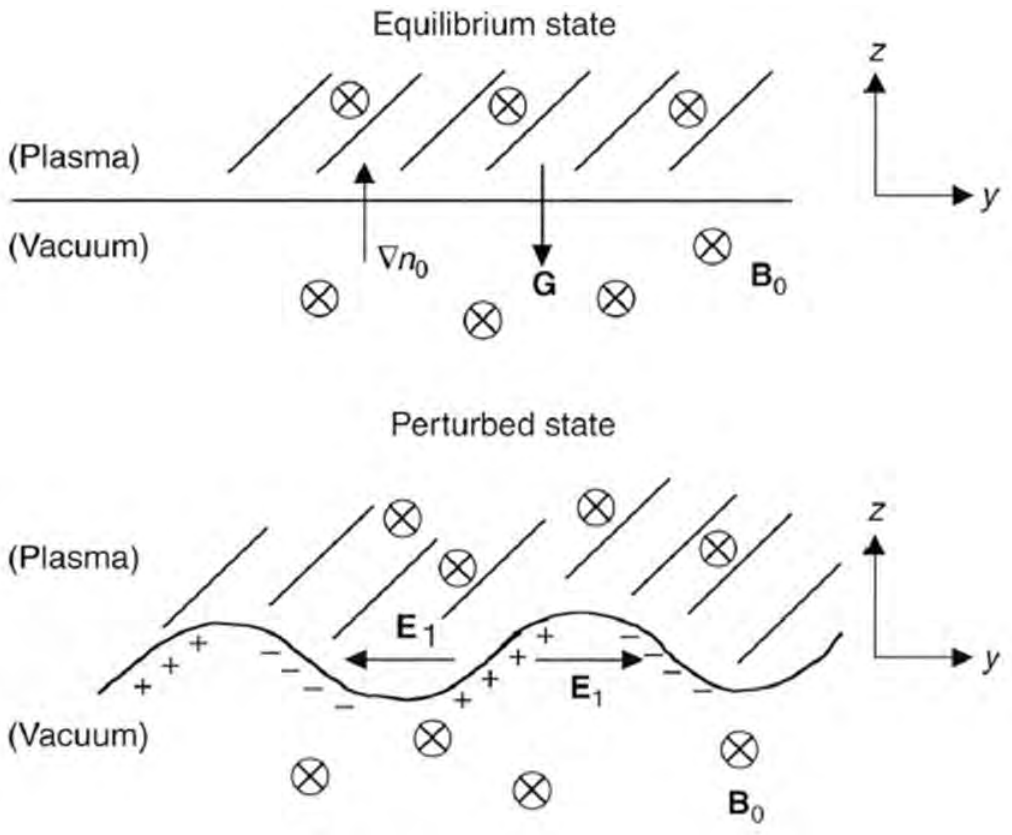

Figure 2. Rayleigh-Taylor Instability configuration. X points to the south, y points to the east, and z points upward. Adapted from Schunk and Nagy, 2009.

Plasma bubbles typically form at 2000 LT and remain as a density depleted region through 2400 LT. Bubbles can also last throughout the night until 0600 LT when sunlight replenishes the plasma in the F layer (Li et al, 2009). Plasma within the bubble is typically depleted by a factor of about 10, but factors of 100 and 1000 and also fairly common (Schunk and Demars, 2003).

Plasma bubbles have been observed to reach altitudes greater than 1500 km and have zonal widths of several hundred kilometers (Sahai et al, 2000). The zonal distance between bubbles is on the order of the bubble width and has been recorded between 400 and 1600 km. Plasma bubbles have been shown to have both eastward and westward

tilts, up to 15 degrees, with height (Sinha and Raizada 2000). Additionally, bubbles have been recorded corotating with the Earth while others super-rotate with speeds up to 3 km/s (Schunk and Demars, 2003).

Table 1 summarizes plasma bubble characteristics.

2.3 Inferring TEC from GPS Measurements

Data collected from a continuously operating global network of Global Positioning System (GPS) receivers can be used to produce global maps of ionospheric total electron content. The GPS network consists of hundreds of dual frequency geodetic quality receivers and 31 GPS satellites. Each GPS receiver tracks between 4 and 12 satellites simultaneously over a site. The TEC in the line of site between the ground station and satellite can be computed using information carried in the GPS signal (Mannucci et al, 1998).

The GPS receivers in the global network generate two delay observables for each satellite being tracked, pseudorange delay and carrier phase delay. Each observable is acquired at the two GPS transmission frequencies, f1 (1.5754 GHz) and f2 (1.2276 GHz).

Table 1. Plasma Bubble Characteristics. Adapted from Nava, 2011.

Characteristic	Typical Values
Depletion Extent	Factor of 10, 100, 1000
N-S Extent	Several thousands of km
Width	Several hundreds of km
Apex Height	≥ 1500 km
Start Time	2000 LT
Dissipation Time	0600 LT (sunrise)
Upward Drift	100 to 500 m/s (slow) 500 m/s to 5 km/s (fast)
Eastward Drift	40-190 m/s
Tilt	10-15 degrees to the west

The frequency differenced phase delays provide very precise measurements of TEC changes but contain an overall bias associated with integer cycle ambiguities. The frequency difference pseudorange data provide an absolute measure of the total ionospheric delay between the satellite and receiver but have significantly more noise than the phase based data. In addition, biases are created by delays in the satellite and receiver hardware (Mannucci et al, 1998).

A TEC observable is formed from the frequency differenced phase delay by adjusting its level based on the pseudorange delay. The TEC observable for each measurement is the phase based ionospheric delay added to the bias. One nanosecond of delay corresponds to 2.85 TEC units (Mannucci et al, 1998).

Vertical TEC is produced from a slant TEC observation measured from the satellite to the ground station. The calculation utilizes a fictitious ionospheric pierce point defined by the intersection of the satellite-receiver line of sight with a thin spherical shell surrounding the Earth, often at an altitude of 450 km. The location of this point is then dropped vertically in altitude to the Earth's surface where it is assigned a latitude-longitude location. The latitude-longitude location of the vertical TEC observation will necessarily differ from the location of the ground station for all elevation angles less than 90 degrees. Figure 3 shows the maximum radial distance possible for a vertical TEC measurement from the associated ground station for several locations worldwide (Mannucci et al, 1998).

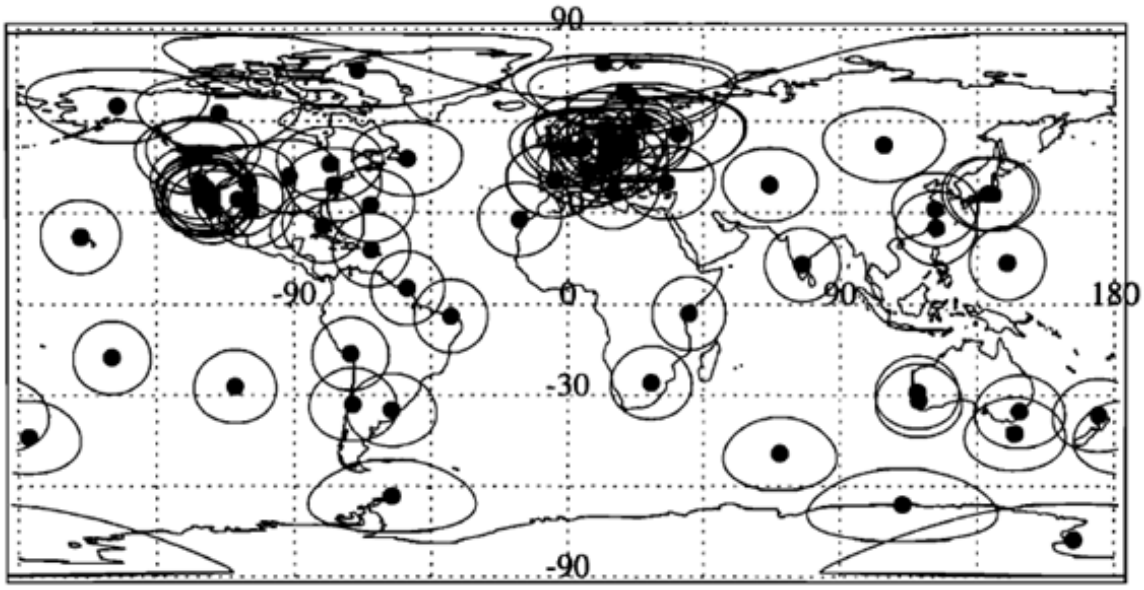

Figure 3. A distribution of GPS ground stations. Ellipses surrounding each ground station represent the maximum distance a vertical TEC observation will be placed from the ground station, assuming an ionospheric shell pierce point of 450 km. From Howe and Runciman, 1998.

2.4 Global Assimilation of Ionospheric Measurements (GAIM) Model

GAIM is a physics-based data assimilation model of the ionosphere developed by the Center for Atmospheric and Space Sciences at Utah State University (USU). At present the USU team has fielded GAIM Gauss-Markov (GAIM-GM), using the Ionospheric Forecast Mode (IFM) as a background model, as the operational Air Force ionospheric model at the Air Force Weather Agency. USU is currently developing GAIM Full Physics (GAIM-FP) which uses the Ionosphere-Plasmasphere Model. GAIM-GM utilizes a Gauss-Markov Kalman filter to ingest ionospheric observations and weight the observations against the IFM background density. Ionospheric observations from several different sources are able to be assimilated and GAIM-GM can be expanded to include a larger network of measurements (Schunk et al, 2004).

GAIM-GM combines a physics based model, the IFM, with ionospheric observations. The ionospheric observations can include in situ electron densities from satellites, bottomside electron density profiles, GPS TEC measurements, satellite occultations, and nighttime UV radiances. Of these observations, GPS TEC measurements and ionosondes are the most commonly used, with the GPS TEC measurements representing the bulk of the ingested data. A Kalman filter is used to assign weights to the relative accuracies of the observations and model inputs. The data is then processed to reconstruct an output of the ionosphere. The outputs of GAIM-GM include a three dimensional electron density, TEC, NmF2, and HmF2. GAIM-GM produces these outputs in user specified global or regional windows with a grid system of 44 nodes meridionally and 24 nodes zonally. In the global mode resolution is 4.67 degrees of latitude by 15 degrees of longitude while the finest regional resolution is 1 degree of latitude by 3.75 degrees of longitude. Boundary conditions for the regional run of GAIM-GM are set from the output of a prior global GAIM-GM model run with the same geophysical conditions (Schunk et al, 2004).

GAIM-GM uses calculated GPS satellite and ground station biases to correct GPS TEC measurements. Each GPS satellite and ground station has a known bias measured in nanoseconds, resulting from satellite drag and clock differences. Also, an error is calculated and associated with each satellite and ground station regarding the precision of the measurement (Schunk et al, 2004).

Additionally GAIM-GM includes several parameters that can be set by the user prior to each run. The time constant is the relaxation time the model uses to decay perturbations to zero. The time constant can be changed along an integer range from 1 to

12 hours and the default is 5 hours. GAIM-GM moves perturbations sun synchronously and the effect of lowering the time constant is to reduce to westward extent the perturbation field will take to relax to zero. The latitude correlation describes the meridional distance the perturbation field is allowed to extend. The latitude correlation can be adjusted along integer values from 2 to 10 degrees and the default value is 10 degrees. Decreasing the latitude correlation lowers north-south distance of the perturbation field (Scherliess et al, 2006).

2.4.1 IFM

The IFM is a physics-based numerical model of the global ionosphere that calculates three dimensional, time dependent density distributions for four major ions (NO^+, O_2^+, N_2^+, O^+) at E region altitudes, two major (O^+, NO^+) and two minor (N_2^+, O_2^+) ions at F region altitudes. Additionally the IFM calculates ion and electron temperatures at both E and F region altitudes as well as H^+ densities in the F region and topside ionosphere. The primary output of the IFM is a three dimensional electron density ranging in altitude from 90 to 1600 km with a resolution of 4 km in the E region and 20 km in the F region. The output density has a 3 degree latitude resolution and a 7.5 degree longitude resolution (Schunk et al, 2004).

IFM inputs include F10.7, year, day, start time, duration of model run, and the temporal variation of Kp from 3 hours prior to the start time through the end of the model run. The IFM is based on a numerical solution of the ion and electron continuity, momentum, and energy equations. The model is able to account for the following physical processes: 1) field-aligned diffusion due to density and temperature gradients,

gravity, and the ambipolar electric field; 2) cross-field electrodynamic drifts due to both magnetospheric and dynamo electric fields; 3) ion production due to UV and EUV solar radiation, starlight, and auroral electron precipitation; 4) numerous energy-dependent chemical reactions; 5) thermospheric winds; 6) neutral composition changes; 7) a myriad of elastic and inelastic heating and cooling processes. Additionally IFM accounts for the offset between the geographic and geomagnetic poles (Schunk et al, 2004).

2.4.2 Kalman Filter

Howe and Runcimen demonstrated the practicality of using GPS TEC measurements within the context of a Kalman filter to produce four dimensional maps of the ionosphere (1998). The Kalman filter is a well established least squares procedure. The filter provides an optimal method for assimilating many different data types into a time-dependent model. The specification of error covariances for the model and observation error is critically important to the proper functioning of the filter. The Kalman filter utilizes a series of six equations to minimize the error at each time step. A forecast is made of the model state, the ionosphere, using Equation 1. The state vector **x** is made by linearly relating the state vector at a time $t + 1$ to the state at the previous time step t through the transition matrix **M**, where η is in the model error. The model state at the new time step is linearly related to the model state at the previous time step through a transition matrix and a forcing term. A forecast model state estimate comes with the forecast model state error covariance, Equation 2, which depends on the previous error and the model error. All information about the model state error is carried forward from one time step to the next by the model error covariance matrix **P** and no information older

than one time step is explicitly retained. The transition model error covariance is given by matrices **Q** and **R**. Measurements $\mathbf{y^o}$ are represented by Equation 3, where **H** is the measurement matrix and ε is the observation error. The model state forecast is combined with the data using the Kalman gain matrix **K**, given in Equation 4, to produce the analysis model estimate, Equation 5, which is the optimal model state estimate given a knowledge of the model state and the data and model error covariances. Equation 6 produces the analysis model error covariance which is reduced from the forecast error by an amount related to the resolving power of the data (Howe and Runcimen, 1998).

$$\boldsymbol{x^f = Lx + \eta} \tag{1}$$

$$\boldsymbol{P^f = LPL^T + Q} \tag{2}$$

$$\boldsymbol{y^o = Hx + \varepsilon} \tag{3}$$

$$\boldsymbol{K = P^f H^T (HP^f H^T + R)^{-1}} \tag{4}$$

$$\boldsymbol{x^a = x^f + K(y^o - Hx^f)} \tag{5}$$

$$\boldsymbol{P^a = (I - KH)P^f} \tag{6}$$

GAIM-GM uses a Gauss-Markov Kalman filter to assimilate ionospheric observations with IFM background states. The background ionospheric density is obtained from the IFM's electron density output while ionospheric measurements are assigned to the perturbation density. The Kalman filter applies the calculated perturbation density to the background density to output a solution for each grid location, according to Equations 7 and 8.

$$N = N_{IFM} + N_{pert} \tag{7}$$

$$N_{pert}^{t+1} = \boldsymbol{L} N_{pert}^{t} \tag{8}$$

A transition matrix **L** is used by the filter at each time step to propagate perturbations forward through time, described in Equation 8. The transition matrix has translation and decay components included. Perturbations move forward in a magnetic sun-synchronous frame and decay towards a value of zero according to a relaxation parameter (Scherliess Et Al., 2006).

The Kalman filter also incorporates a model error covariance matrix, used to estimate the uncertainties in the model state which is the perturbation field. The model error covariance matrix has been predetermined from 1107 individual two-day runs of the IFM that spanned a range of ionospheric forcing conditions. The filter also applies correlations in both the zonal and meridional directions. Zonal correlation are tied to the time constant while meridional correlations are set by the latitude correlation (Scherliess Et Al., 2006).

The five types of observations the Kalman filter in GAIM-GM can ingest are TECs from GPS, ionosondes, in situ electron densities, electron density profiles from ground based radars, and optical emission profiles. The most common data types used by GAIM-GM are GPS TEC measurements and ionosondes (Thompson et al, 2006).

III. Methodology

This chapter describes the methodology used in conducting the research. The first section discusses the plasma bubble structure and placement. Then the calculation of slant TEC and generation of GPS files is covered. The next section details adjustments and considerations within GAIM-GM to include station and satellite biases, the plasmasphere, the time constant, and the latitude correlation. Finally, the conditions GAIM-GM was tested under are outlined.

3.1 Generating Plasma Bubble Observations

First, a method to input plasma bubble observations into GAIM-GM was developed. GAIM-GM uses the IFM background state modified by GPS slant TEC data. The IFM is a physics-based model that accounts for the date, solar, and geomagnetic conditions. The IFM does not use ionospheric observations and does not contain the necessary physics to model plasma bubbles. GPS slant TEC data are measurements of the ionosphere calculated from the phase delay of signals from GPS satellites. Of these two data sources into GAIM-GM, real-world plasma bubble observations would be present in the GPS slant TEC data. Consequently utilities were developed to place plasma bubble observations into synthetic GPS slant TEC data.

In order to isolate the effect of plasma bubbles on GAIM-GM output, it is necessary to have consistency between the IFM and GPS slant TEC inputs. If the GPS measurements differ from the IFM background state the Kalman filter will introduce perturbation fields to reconcile the differences. The perturbation fields have far reaching effects in the model grid due to the time constant and latitude correlation, hindering any

plasma bubble signature. Therefore the IFM electron density field was used as the background from which to construct artificial GPS slant TEC data. Slant TECs were calculated through the IFM electron density both with and without bubbles present. The slant TECs calculated with bubbles absent created a set of measurements identical to the IFM background state used by GAIM-GM, limiting the presence of perturbation fields. GAIM-GM was then run using slant TEC measurements with bubbles present to be evaluated against the bubbles absent case. Both IFM and slant TEC files were provided to GAIM-GM in 15 minute increments for each model day.

3.1.1 Plasma Bubble Structure

Plasma bubbles were imposed upon the IFM electron density field according the method described by Nava (2011). First, the original resolution of the IFM electron density grid was doubled to produce a grid with 3.75 degree longitudinal and 1.5 degree latitudinal spacing. The variable spacing between the altitude grid points was halved in order to double the vertical resolution. The electron densities were linearly interpolated to determine their values at the newly created IFM grid points. The grid resolution was increased to create plasma bubbles of a realistic size. Figure 4 prescribes the method to measure bubble width in the modified IFM electron density grid. Because slant TECs calculated through the grid take an average of the nearest eight grid points in three dimensional space, the effective width of the bubble spans from one undepleted column of grid points, across the depleted column, and to the next undepleted column of grid points. For the modified IFM grid with 3.75 degrees between grid points the result is a bubble width of 7.5 degrees, a large width for a plasma bubble but still physically

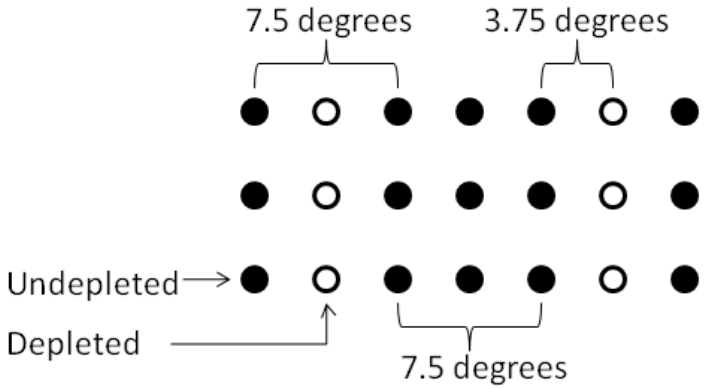

Figure 4. Depletion width of a plasma bubble in the modified IFM electron density resolution. Adapted from Nava, 2011.

reasonable. In the original 7.5 degree longitudinal resolution of the IFM, a bubble width would be 15 degrees, too wide to be physically reasonable and necessitating the modification to increase the IFM resolution (Nava 2011).

Next, specific grid points were chosen to form the outline of the plasma bubble. The bubble was shaped like an upside down watermelon slice elongated along Earth's magnetic field lines. The base meridional length of the bubble was specified, from which the apex height of the bubble is calculated from Equation 3,

$$r = R_0 sin^2\theta \qquad (3)$$

where r is the dipole field line radius, θ is the colatitude, and R_0 is the radial distance to the point where the dipole field crosses the geomagnetic equator. The electron density at each chosen grid point was then divided by the specified depletion factor. A side view of a plasma bubble in the IFM electron density is shown in Figure 5 (Nava 2011).

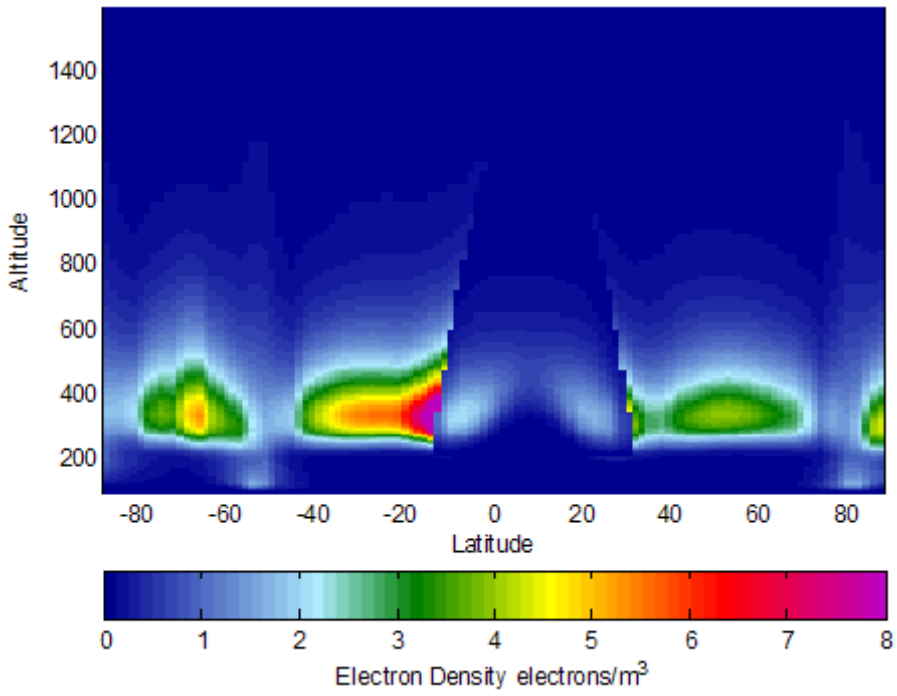

Figure 5. Longitudinal view of a plasma bubble in the IFM electron density grid. Scale is in units of electrons per square meter.

3.1.2 Plasma Bubble Placement

Although plasma bubbles have been observed globally across the equatorial regions of the Earth it was decided to focus on bubbles occurring over the South American sector. South America contains the highest density of equatorial ground stations and provides a distribution that has a large latitudinal extent. Plasma bubbles were imposed on the IFM electron density grid over South America. The bubbles were formed at 2000 LT and removed at 0600 LT to match typical characteristics. Because the bubble upward velocity during its formation can be large, the 15 minute time resolution of the IFM is less than the time it takes a bubble to rise from 200 to 1400 km, therefore a bubble appears in its full form from one IFM time step to the next. Bubbles were placed 7.5 degrees apart as measured from edge to edge and shown in Figure 4. When a

sequence of bubbles was used, each bubble would form at 2000 LT for its longitude and the next bubble would form 7.5 degrees to the west one hour later. Once a bubble has formed, three different methods of movement were modeled to test GAIM-GM. The first method kept the bubbles corotating with the Earth, a common characteristic of bubbles, shown in Figure 6. Some bubbles super-rotate which led to a second condition where the bubbles would form at 2000 LT and then allowed to super-rotate at 230 m/s, or 7.5 degrees/hr, depicted in Figure 7. Figure 8 is the third and unrealistic case, with the bubble moving sun synchronously to highlight the performance of the time constant.

3.1.3 Slant TEC calculation

With the depleted region representing the plasma bubble placed in the electron density grid the following step was performed to calculate slant TECs through the artificial ionosphere. The method for calculating slant TEC was described by Nava and is an adaptation of the code generated by USU. The code creates a linear path between the satellite and ground station and places this path in the context of the IFM electron density grid. Points are selected every 5 km along this path where the 8 nearest grid points, three dimensionally, are linearly interpolated to construct a representative electron density for the path point. The path points are then summed and a conversion factor is applied to change from electron density to the path integrated TEC. The calculated TEC thus represents the TEC through the IFM electron density grid along the path from the satellite to the ground station (Nava 2011).

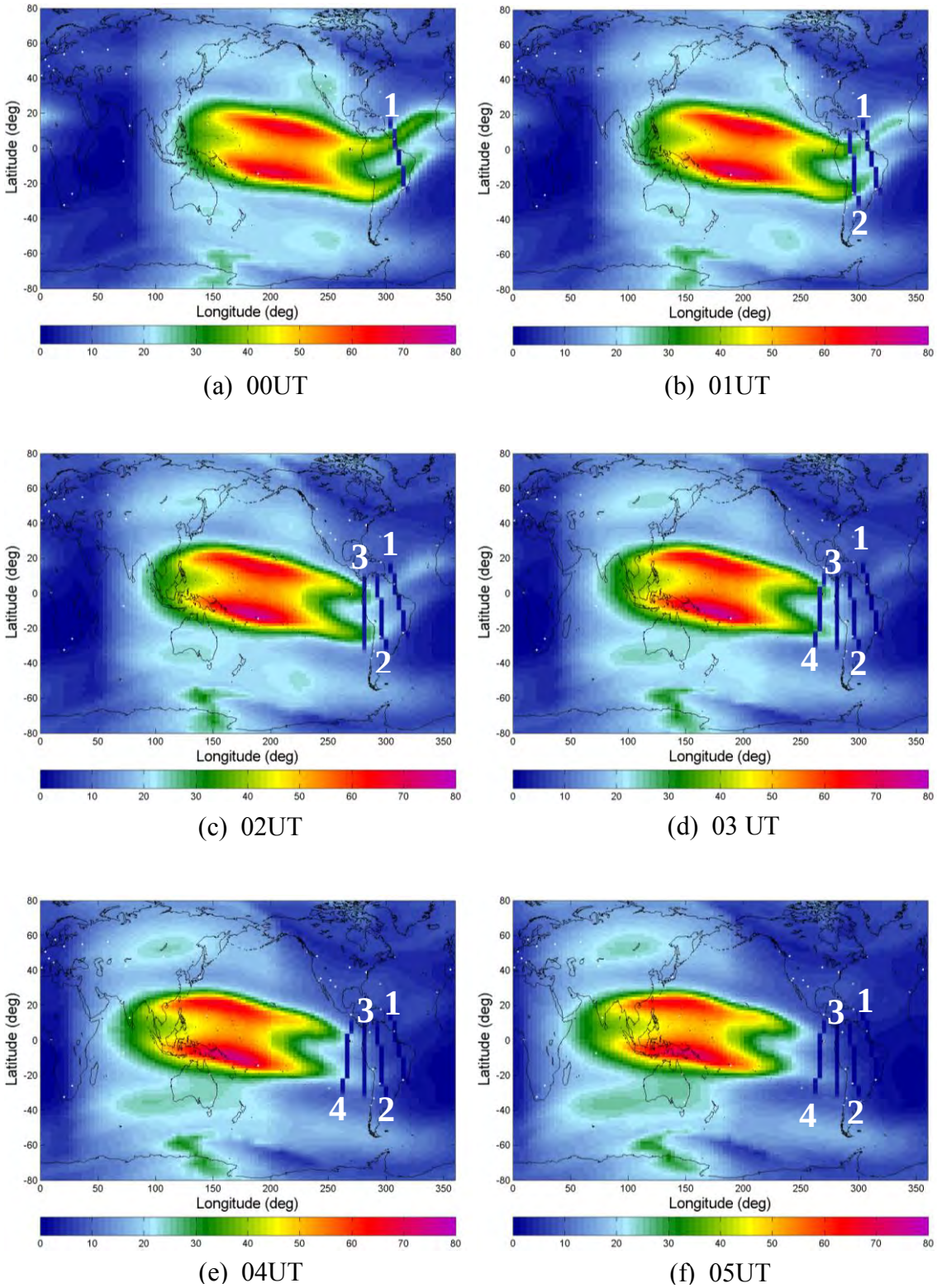

Figure 6. Formation of 4 corotating plasma bubbles for day 82, F10.7 = 113 SFUs. Bubbles are placed in modified IFM electron density grid and numbered according to formation order. Units are in TEC electrons per square meter.

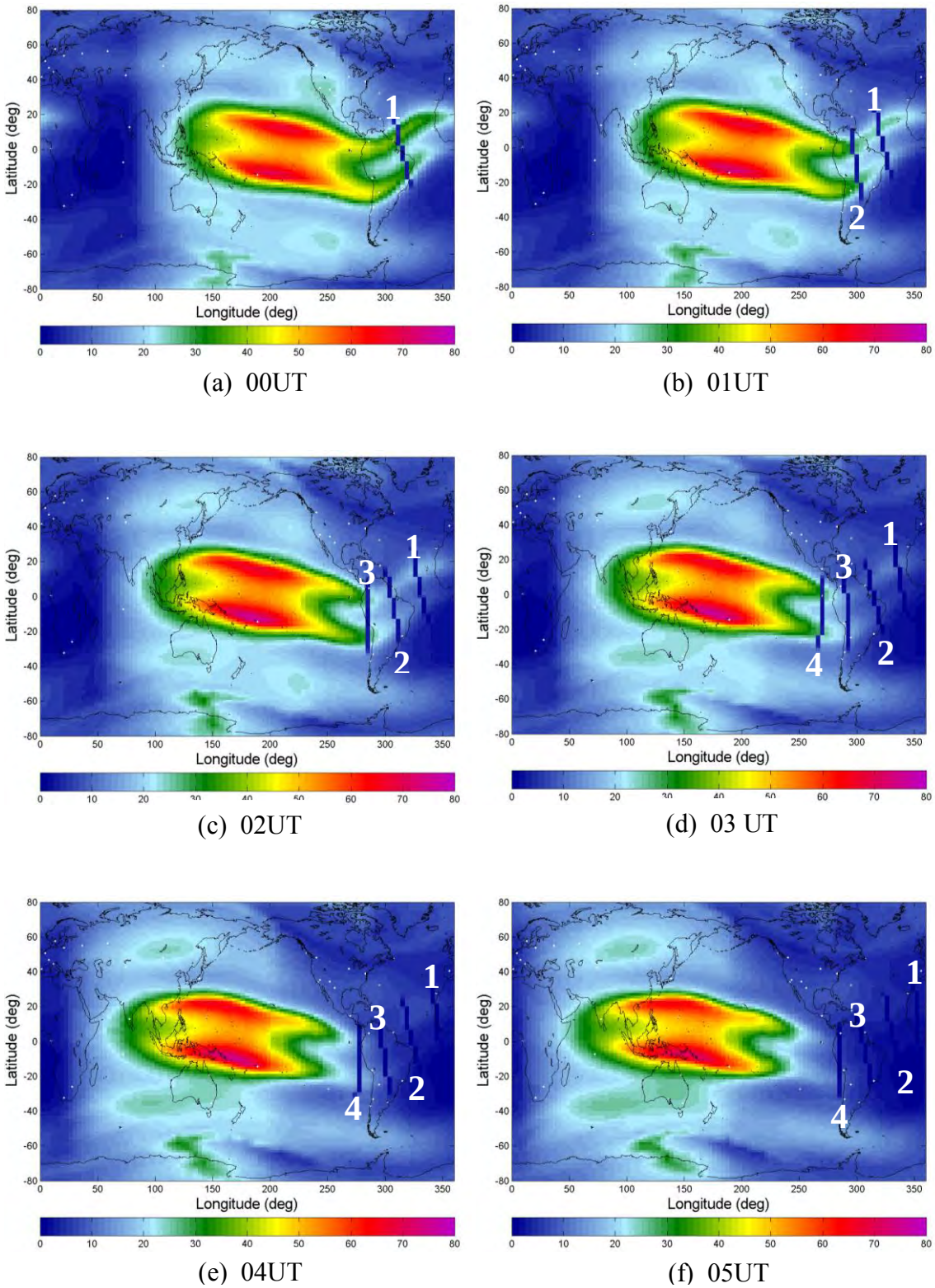

Figure 7. Evolution of 4 super-rotating bubbles for day 82, F10.7 = 113 SFUs. Bubbles placed in modified IFM electron density grid and numbered according to order while moving east at 230 m/s. Units are in TEC electrons per square meter.

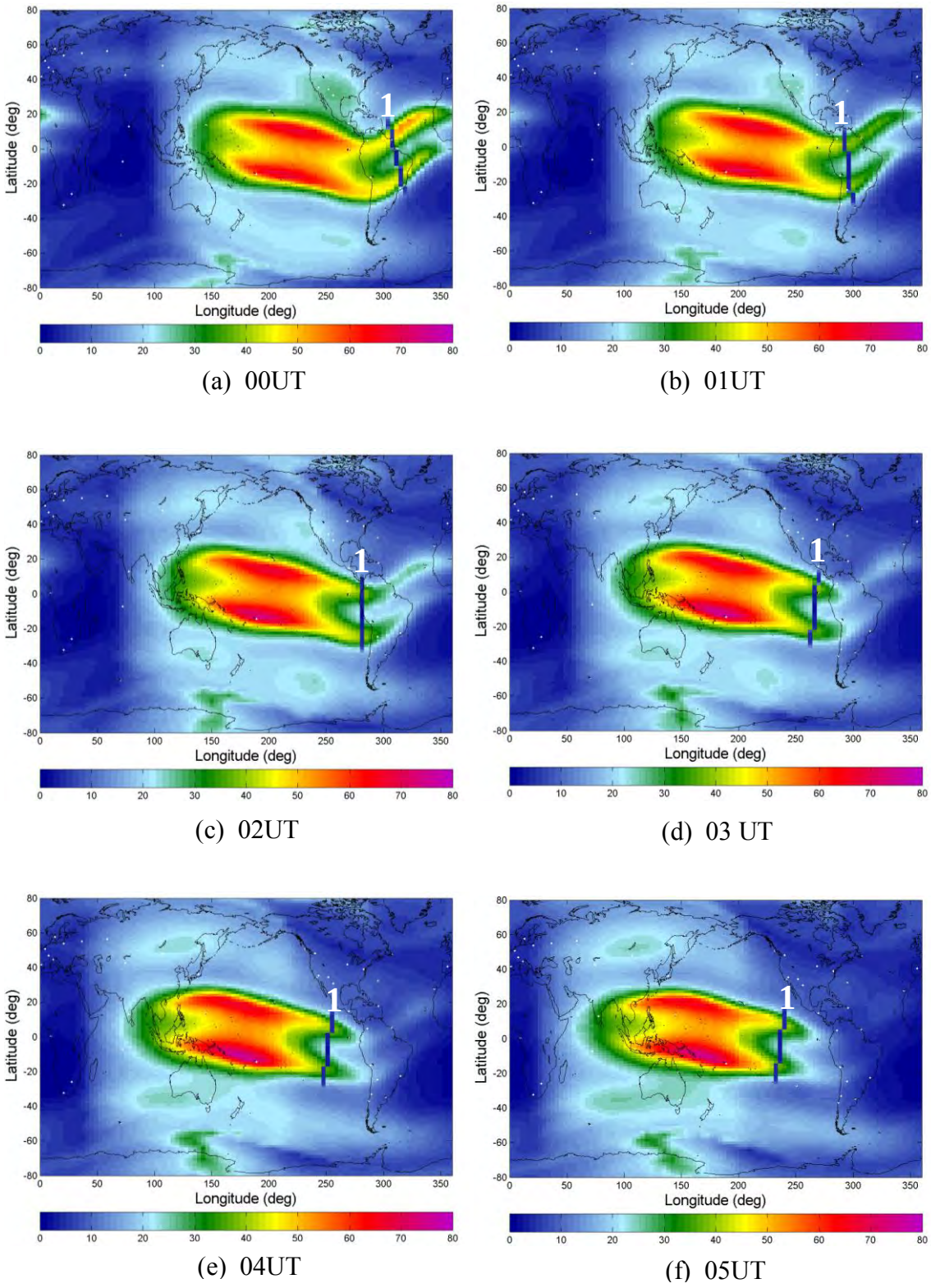

Figure 8. Evolution of 1 sun synchronous bubble for day 82, F10.7 = 113 SFUs. Bubble placed in modified IFM electron density grid. Units are in TEC electrons per square meter.

3.1.4 GPS Input Files

GPS files are ingested by GAIM-GM and reduced to a readable format for the model. Each GPS file contains the data from one ground station for a one hour time period. The data is organized into 22 columns which include time, date, satellite identification information, look angle data, derived TEC data, satellite location, and ground station location. GAIM-GM uses the date, time, satellite identification, satellite location, ground station location, TEC, and TEC error when ingesting GPS observations. New GPS files were written as text files in MATLAB into the format expected by GAIM-GM. Time, date, satellite identification, satellite location, ground station location, TEC, and TEC error were all specified for each GPS file. The TEC error was set at 3 TECU to allow for differences in representativeness of a given slant path through the modified electron density grid. Finally, the computed TEC value from the modified electron density grid was written to the file. GPS input files were created every hour for each ground station. Each ground station observes between 5 and 10 satellites at each time step with position and TEC calculated at 15 minute increments. GPS files were translated into reduced .gps format that is readable by GAIM-GM. The files were then transferred to the GAIM-GM GPS directory to be ingested into the model.

3.2 GAIM Adjustments

3.2.1 Satellite and Station Biases

GAIM-GM corrects the GPS TEC measurements for known satellite and ground station biases. Under normal operation the satellite and ground station biases are downloaded from an archive at the University of Bern in Switzerland. Each file contains

the monthly bias and root mean square uncertainty of the bias, both expressed in nanoseconds (GAIM 2010). Because this research is using synthetic GPS files, historic satellite and ground station biases do not apply. In real GPS measurements it is necessary to have a satellite and ground station bias adjustment to account for measurement error, but since the calculation through the IFM's electron density does not use equipment to observe the TEC, the measurement is exact and the satellite and ground station biases are zero. The slant TECs calculated are an exact solution because the IFM creation of the ionosphere used to derive the TEC measurement is a known quantity. For the purposes of this study both the satellite and ground station biases were set at a nominal value of 0.001 ns, the lowest value accepted by the model.

3.2.2 Plasmasphere

In addition to the satellite and ground station biases, GAIM-GM accounts for the TEC contribution from the plasmasphere in its use of GPS files. Because GAIM-GM calculates an electron density from 90 to 1380 km and satellite observations measure the entire TEC from satellite to ground station, TEC from 1380 km and upwards in the plasmasphere must be subtracted from the GPS TEC observation to provide GAIM-GM with a TEC specific to its altitudes. Again, in this study the slant TECs used in the GPS files were generated from the modified IFM electron density grid from 90 to 1598 km. Thus there is no plasmasphere contribution in the GPS file TEC measurement and no need to subtract this quantity from the TEC contained in the GPS input files. USU provided a flag in the GAIM-GM startup file that removed the subtraction of the

plasmasphere within GAIM-GM, which allows the Kalman filter to receive the appropriate TEC value for this study.

The slant TEC path through the IFM is calculated for IFM altitudes from 90 to 1598 km. The top altitude of GAIM is 1380 km, leaving a 218 km difference between the tops of the two models. When GAIM-GM makes its usual plasmasphere correction the model subtracts the electron density contribution from 1380 km up to the satellite orbit. Slant TECs used in this study were derived from the IFM, meaning an extra contribution of electron density was added from 1380 km to 1598 km. As part of this research, a study quantified the TEC contribution from 1380 to 1598 km in the IFM. It was found that this 218 km layer contributes a maximum value of 0.23 TECU in the dayside, midlatitude ionosphere and 0.05 TECU in the nightside, equatorial ionosphere. Because the TEC contribution from this layer is small compared to the background TEC values, the effect is assumed to be negligible and was not corrected.

3.3 Running the Models

The IFM is an input to GAIM-GM and must be run prior to GAIM-GM. The IFM requires a 24 hour model time warm up prior to producing useful output. The IFM was run for two day series' to construct a useable input for GAIM-GM. The first day of each series was discarded as a warm up day and the second day was used for input to GAIM-GM. For example, to create useable IFM output for GAIM-GM for days 81 and 82, 2-two day runs of the IFM were completed. The first IFM run was for days 80 and 81 and the second IFM run was for days 81 and 82. In each of these runs the second day of

output was used as the input to GAIM-GM making a useable set of IFM files for days 81 and 82.

GAIM-GM also requires a warm up day to create correct ionospheric output. For example, to create output for day 82 GAIM-GM was run for days 81 and 82. This requires IFM and GPS input for both days. For runs containing bubble observations in the GPS files, the second day of input files contained slant TEC values from the IFM with bubbles present while the first day was composed of slant TEC values from the IFM without bubbles. For cases involving a regional GAIM-GM the model must previously be run globally to create boundary conditions. The global output boundary conditions were created from GAIM-GM without GPS inputs present.

3.4 Results Analysis Format

The results in this paper are presented three formats: GAIM-GM TEC output, percent difference maps, and skill scores. The GAIM-GM TEC output is a display of the TEC in longitude and latitude coordinates. The percent difference maps show a quantitative representation of the spatial extent of the plasma bubble depletions in GAIM-GM. The skill scores yield a numerical representation of the relative accuracy of the GAIM-GM representation compared to climatology.

3.4.1 Percent Difference Maps

The percent difference map is the primary method of data representation in this paper. To create the difference, two TEC outputs from GAIM-GM must be generated. A percent difference is calculated for each grid point in the GAIM-GM output using Equation 4.

$$Percent\ difference = \frac{TEC\ output\ A - TEC\ output\ B}{TEC\ output\ B} * 100 \quad (4)$$

TEC output A and B represent the experiment and control cases, respectively. For example, to show the effect of bubbles on the TEC, the model output with bubbles present would be assigned to A and the output with bubbles absent to B. Since bubbles are depleted TEC values within the ionosphere, a negative percent difference indicates the presence of plasma bubbles in the GAIM-GM output because B, the control case with bubbles absent, would be larger than A, the experiment with bubbles present. The percent difference output is then plotted against the latitude and longitude axes with a world map overlay. Percent difference is a more meaningful calculation than a regular difference between the TEC outputs because the percent difference contains information about the control state of the ionosphere and how much deviation the experiment state of the model has changed. For a depletion factor of 10 the percent difference from the control TEC output would ideally be 90%, a factor of 100 would be 99%, and a factor of 1000 would be 99.9%. Percent difference maps allow for a quick analysis of the accuracy of depletion magnitude.

3.4.2 Skill Scores

Skill scores were utilized as a method to objectively evaluate the performance of GAIM-GM. A skill score is composed of three inputs, a reference, an observation, and a tested parameter. The reference is the climatology, in this case the GAIM-GM output with bubbles absent. The IFM TEC output with plasma bubbles imposed was used as the observation or truth. The tested parameter was the GAIM-GM output constructed with

GPS input files having bubbles present. A skill score is the ratio of the root mean square errors of the inputs given by Equations 5, 6, and 7.

$$RMSE = \frac{1}{N}\sqrt{\sum_{m=1}^{N}(Tested\ Parameter_m - Observation_m)^2} \tag{5}$$

$$RMSE_{ref} = \frac{1}{N}\sqrt{\sum_{m=1}^{N}(Reference_m - Observation_m)^2} \tag{6}$$

$$SS = 1 - \left(\frac{RMSE}{RMSE_{ref}}\right) \tag{7}$$

The IFM TEC output grid and the GAIM-GM TEC output grid are different resolutions. In order to use the skill score equations the grids of the three inputs have to match exactly. The solution is to tailor the GAIM-GM regional output area to match the IFM grid locations by adjusting the selected region in the GAIM-GM set up file. The grid used for the regional GAIM-GM output and the skill scores goes from 33S to 10.5N and 240E to 326.25E. The resolution of the output is 1.5 degrees of latitude by 3.75 degrees of longitude, the same resolution as the modified IFM grid. Skill scores range from an upper limit of 1 down through 0 and have no negative bound. A skill score greater than zero means the tested parameter's output was an improvement to the reference compared to the observation. A negative skill score means the tested parameter's output was worse than the reference compared to the observation. Skill

scores closest to 1 are desired. A comparison between two tested parameters can occur if the same reference and observation are used to compute each skill score.

3.5 Test Cases

GAIM-GM was run with and without bubbles present through a range of model parameters, geophysical conditions, and bubble characteristics, presented in Table 2. Model parameters tested included the resolution, time constant, and ground station density. Both the global and regional model resolutions were tested and due to the better performance of the regional mode, most of the remaining test cases were performed in the regional resolution. The default time constant of 5 hours and the minimum of 1 hour were compared in both global and regional resolutions. The AFWA GPS ground stations list and an ideal grid of regionally distributed ground stations were used to test the effect of varying the ground station density. The global distribution of AFWA ground stations is shown in Figure 9 and regionally in Figure 10. The ideal grid of regionally distributed ground stations is presented in Figure 11.

Table 2. List of parameters varied during the assessment of plasma bubble effects on GAIM-GM.

Model Parameters	Geophysical Conditions	Bubble Characteristics
Model Resolution 1) Global 2) Regional	Seasons 1) Spring Equinox 2) Winter Solstice	Factor of Depletion 1) 10 2) 100 3) 1000
Time Constant 1) 5 hours (default) 2) 1 hour (minimum)	Solar Cycle 1) Solar minimum F10.7 = 70 SFUs 2) Solar medium F10.7 = 113 SFUs 3) Solar maximum F10.7 = 210 SFUs	Bubble Movement 1) Co-rotating 0 m/s 2) Super-rotating 230 m/s to the east 3) Sun synchronous 660 m/s to the west
Ground Station Density 1) AFWA Stations 2) Ideal Grid		

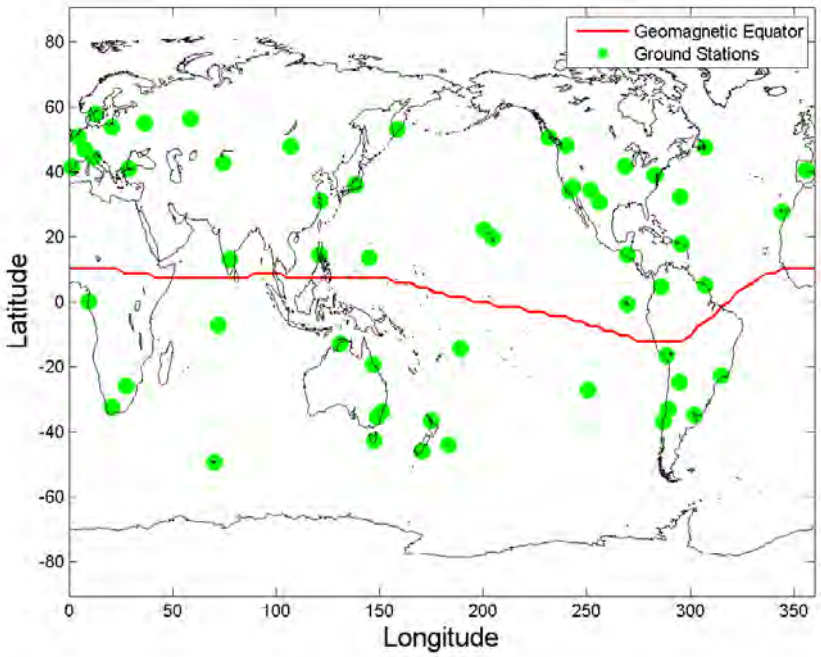

Figure 9. Global distribution of 59 AFWA GPS ground stations.

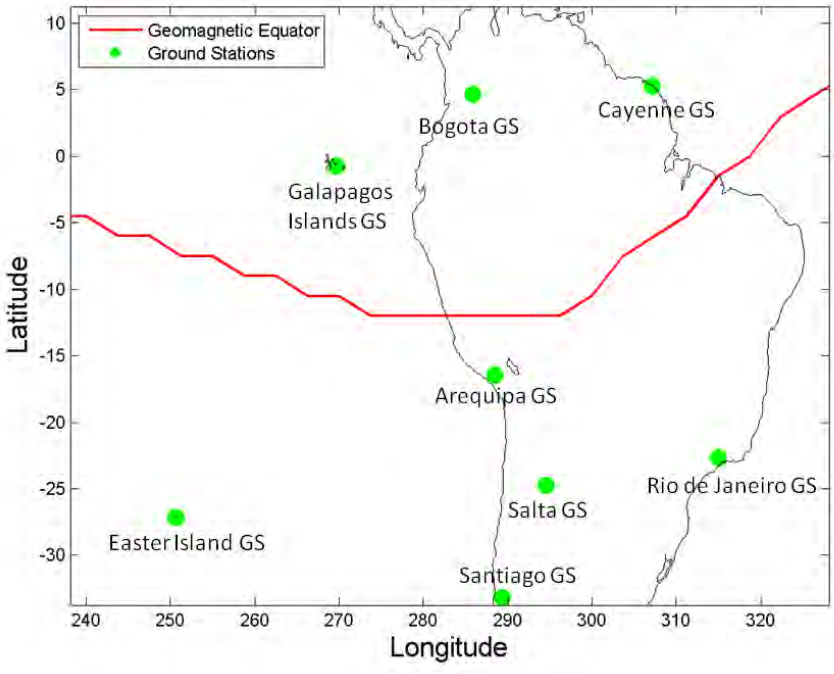

Figure 10. Regional distribution of AFWA station list GPS ground stations.

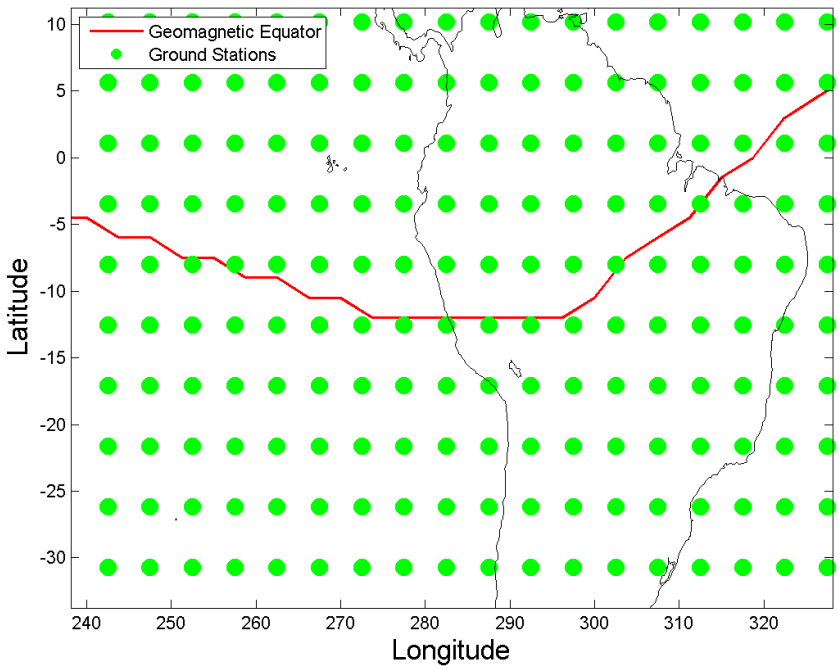

Figure 11. Regional distribution of ideal GPS ground station list.

Next, seasonal and solar cycle changes were made to test geophysical constraints on plasma bubble reproduction in GAIM-GM. The spring equinox and winter solstice of 2004 were chosen for the seasonal comparison. Three solar cycle conditions were studied, solar minimum, medium, and maximum. The three solar states were characterized by their F10.7 values, which are a measure of the solar flux at 10.7 cm, which is used as a proxy for the shorter wavelength flux that produces photoionization in the ionosphere. Solar minimum was defined as an F10.7 = 70 solar flux units (SFUs), solar medium as a F10.7 = 113 SFUs, and solar maximum as a F10.7 = 210 SFUs. Geomagnetic quiet conditions, Kp = 1, were used for the duration of the research.

Finally, depletion factors and bubble movement constituted the plasma bubble characteristics that were tested. Three factors of depletion, 10, 100, and 1000 were used.

Additionally, three methods of bubble movement were studied, co-rotating, super-rotating, and sun synchronous bubble movement. Super-rotating bubbles moved to the east at 230 m/s after their formation at 2000 LT. Although bubbles have only been observed to super-rotate at speeds up to 190 m/s, 230 m/s was chosen as a realistic upper bound that fit well into the modified IFM grid resolution. The sun synchronous bubble movement is physically unrealistic, but provides a test of the perturbation movement assumption built into the Kalman filter by moving a single bubble to the west at 660 m/s, or 15 degrees per hour. Table 3 lists the 18 GAIM-GM runs that were conducted by varying these parameters.

Table 3. Variable matrix for GAIM-GM model runs completed.

Run Number	Day	Mode	Bubble # or type	Depletion Factor	Time Constant	# of Ground Stations	F10.7	Remarks
1	82	global	0	n/a	5	59	113	global control
2	82	global	4 corotate	10	5	59	113	global bubbles present
3	82	regional	0	n/a	5	59	113	regional control
4	82	regional	4 corotate	10	5	59	113	regional bubbles present
5	82	global	4 corotate	10	1	59	113	global time constant = 1
6	82	regional	4 corotate	10	1	59	113	regional time constant = 1
7	356	regional	0	n/a	5	59	113	regional solstice control
8	356	regional	4 corotate	10	5	59	113	regional solstice factor 10 depletion
9	356	regional	4 corotate	100	5	59	113	regional solstice factor 100 depletion
10	356	regional	4 corotate	1000	5	59	113	regional solstice factor 1000 depletion
11	82	global	1 sun synchronous	10	5	59	113	global sun synchronous bubble
12	82	regional	4 super-rotate	10	5	59	113	regional super-rotate bubbles
13	82	regional	4 corotate	10	5	408	113	regional ideal grid bubbles present
14	82	regional	0	n/a	5	408	113	regional ideal grid control
15	82	regional	0	n/a	5	59	70	solar minimum control
16	82	regional	4 corotate	10	5	59	70	solar minimum bubbles present
17	82	regional	0	n/a	5	59	210	solar maximum control
18	82	regional	4 corotate	10	5	59	210	solar maximum bubbles present

IV. Results and Analysis

This chapter will present and analyze the results of placing plasma bubbles into the GPS input files of GAIM-GM. First, GAIM-GM TEC output from both global and regional modes will be compared to show the utility of the regional mode. Next, plasma bubbles with different depletion factors will be evaluated with a focus on the similarities in the results. Seasonal and solar cycle differences will follow emphasizing the impact of the background ionospheric TEC values on GAIM-GM plasma bubble reconstruction. Then, the time constant model parameter will be evaluated by varying the time constant and bubble motion. Finally, the GPS ground station density will be increased to an ideal regional grid to showcase the effect of additional ground stations on plasma bubble recreation.

The results presented in this thesis expand upon an earlier study on the effect of plasma bubbles on the output of GAIM-GM conducted at USU by the Center for Atmospheric and Space Sciences. Drs. Schunk, Scherliess, and Thompson tested the capability of GAIM-GM to model plasma bubbles and storm enhanced density regions in terms of the quantity of GPS observations available to the model (2010). Plasma bubble characteristics and model conditions were duplicated from the USU study to initialize and verify the methods and models used presently. Both the USU and present methodology place four bubbles, each forming at 2000 LT, over South America with factor of 10 density depletions. The only significant difference between the two procedures was the width of the bubbles, which was set at 5 degrees by USU and 7.5 in this paper due to IFM grid spacing. The separation between bubbles in both cases approximated the bubble

width and the same bubble center points were used. Initial output for this study was verified against the USU study for consistency and showed the similar input conditions independently produce comparable results in GAIM-GM output (Schunk et al, 2010). The verification process also included tests of the time constant, latitude correlation, plasmasphere correction, and satellite and station bias correction, all of which performed as expected.

4.1 Global and Regional Resolution Analysis

The longitudinal resolution of GAIM-GM in global mode is 15 degrees which is twice as large as the 7.5 degree plasma bubbles used in this study. Because the model grid resolution is larger than the bubble itself it was anticipated that GAIM-GM would have difficulties reproducing the bubbles, particularly the magnitude of the depletions. GAIM-GM in regional mode has a longitudinal resolution of 3.75 degrees, half that of one bubble width, and therefore was expected to reproduce bubbles better than in global mode. Figure 12 shows GAIM-GM TEC output and percent difference maps for both global and regional model runs. Panels (c) and (d) are GAIM-GM TEC output constructed from input files containing plasma bubbles with a depletion factor of 10. The four plasma bubble structures that were placed into the input files cannot be resolved in either the global or regional resolution TEC outputs. Panels (e) and (f) show that the depletions present in the TEC outputs do not resemble the bubble positions input. Additionally, the magnitude of the depletions is less than 30% which is significantly less than the 90% depletions placed in the input files. The area of the depletion in the global mode is incorrectly distributed zonally, seen in panel (e). The bubbles, as input into

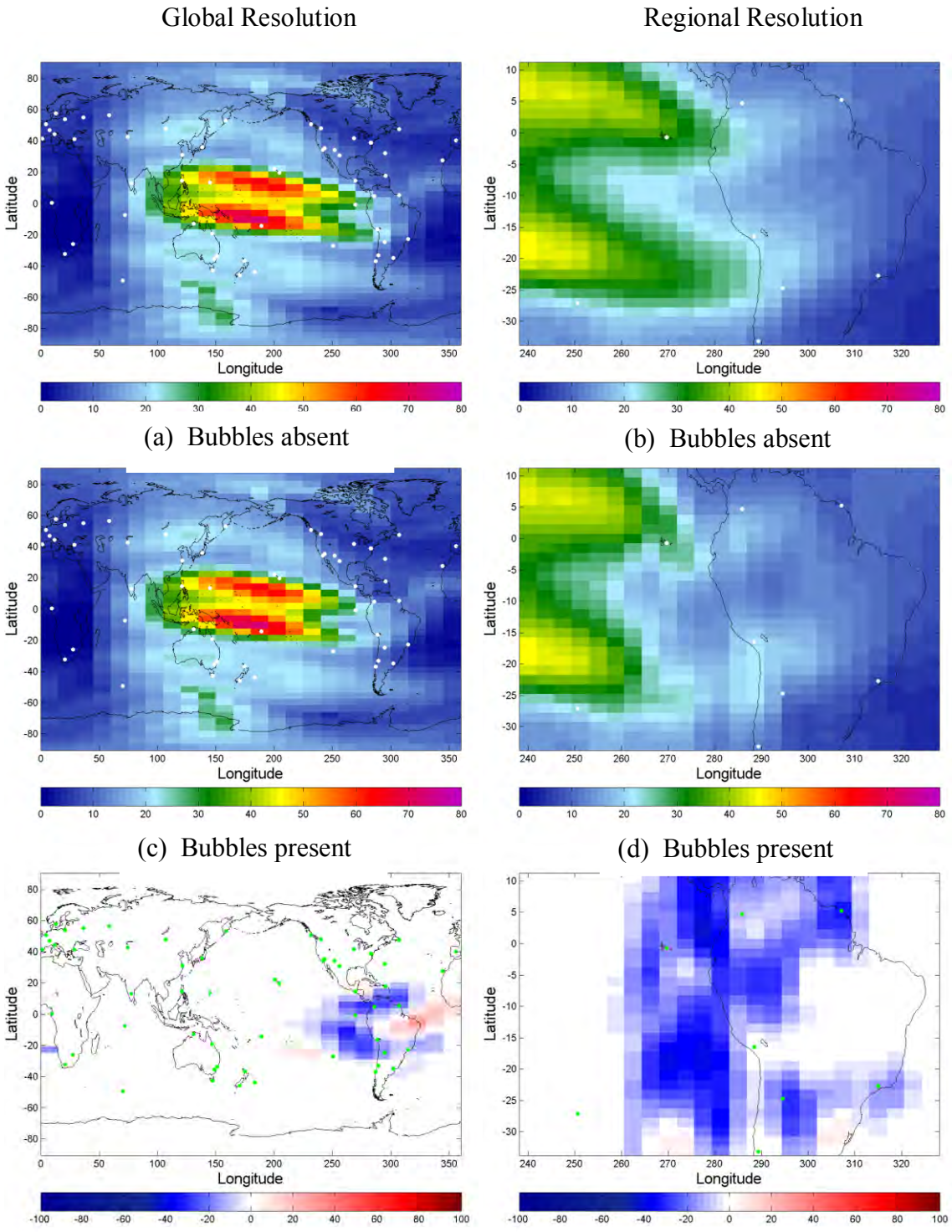

Figure 12. Comparison of GAIM-GM global and regional resolutions. Panels (a) through (d) in units of TEC * 10^{16} electrons/m^2. Panels (e) and (f) are percent differences between the above panels.

GAIM-GM through the GPS measurements, are elongated north to south, previously shown in Figure 6. The regional mode also does not correctly reproduce the bubbles, but is more adept at keeping the bubbles' longitudinal distribution than the global mode. The regional mode outperforms the global mode due to the improved ratio of grid resolution to feature size. Next, regional mode was used to study the effect of depletion magnitude on GAIM-GM output.

4.2 Magnitude of Depletion Analysis

A comparison of depletion factors of 10, 100, and 1000 is presented in Figure 13, again for the case of four plasma bubbles over South America at 03UT. Panels (a), (b), and (c) all look remarkably similar and in fact are within 1.5 TECU, or 10%. The depletions cover a nearly identical area in each case. Panels (d) and (e) confirm that all three outputs for varying depletion factors are within 10% of each other.

The observed result that varying the magnitude of the bubble depletions has little affect on the GAIM-GM output can be explained by an analysis of the Kalman filter present in the model. The Kalman filter in GAIM-GM discards GPS measurements greater than a factor of 5 less than the background ionosphere created from the previous time step. Because different look angles between GPS satellites and ground stations will see varying degrees of the bubble, not all look angles will be passed through the filter. Figure 14 is a layout of three example look angles through a plasma bubble placed in the IFM electron density grid. Look angle 1 does not pass through the plasma bubble and the associated TEC value is unaffected. The second look angle passes partially through the plasma bubble. TEC values resulted from look angle 2 are reduced, but not by enough to

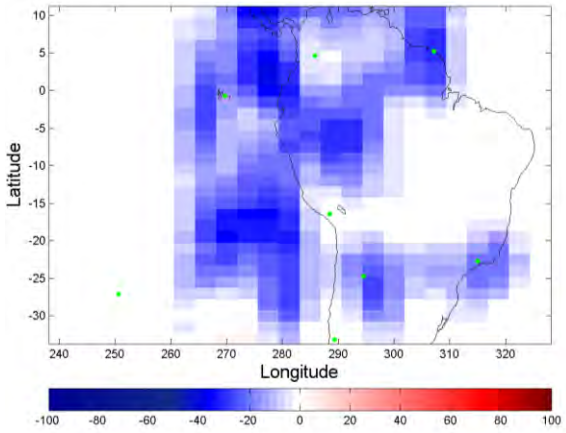

(a) Factor of 10 depletion

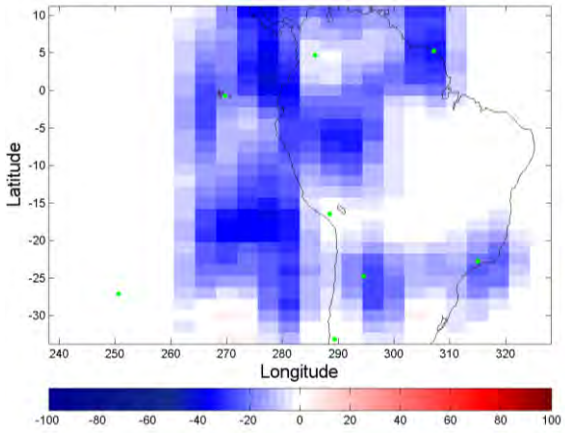

(b) Factor of 100 depletion

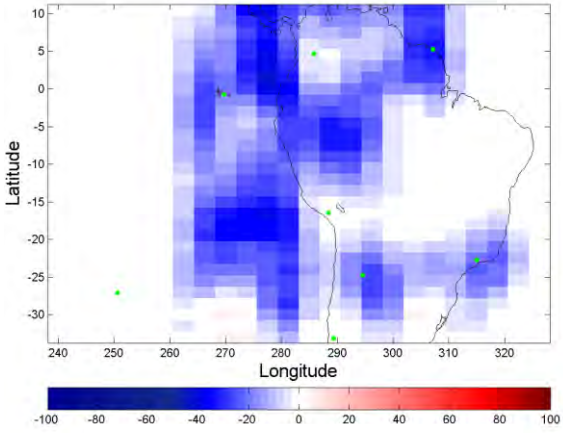

(c) Factor of 1000 depletion

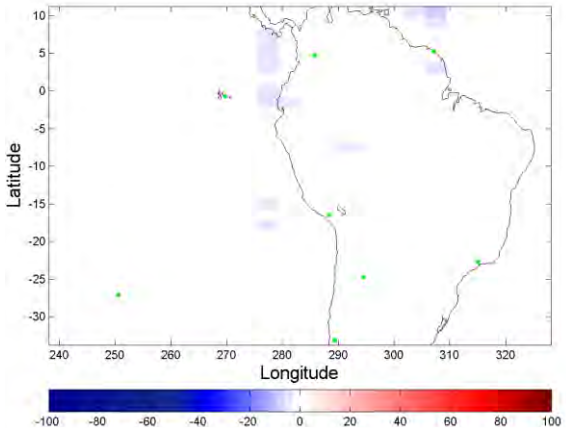

(d) Factor of 100 – factor of 10 depletion

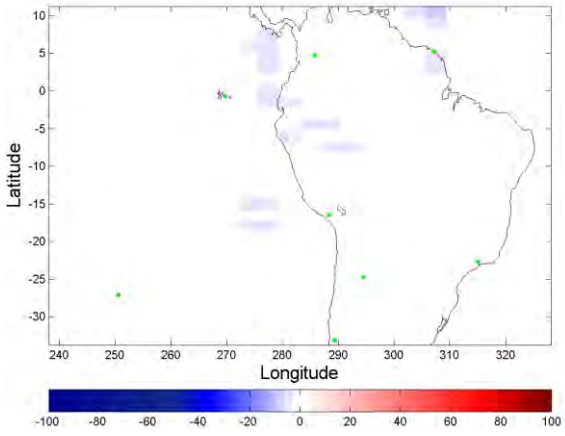

(e) Factor of 1000 – factor of 10 depletion

Figure 13. Percent difference comparison of factor of 10, 100, and 1000 bubble depletions. Valid at 03UT.

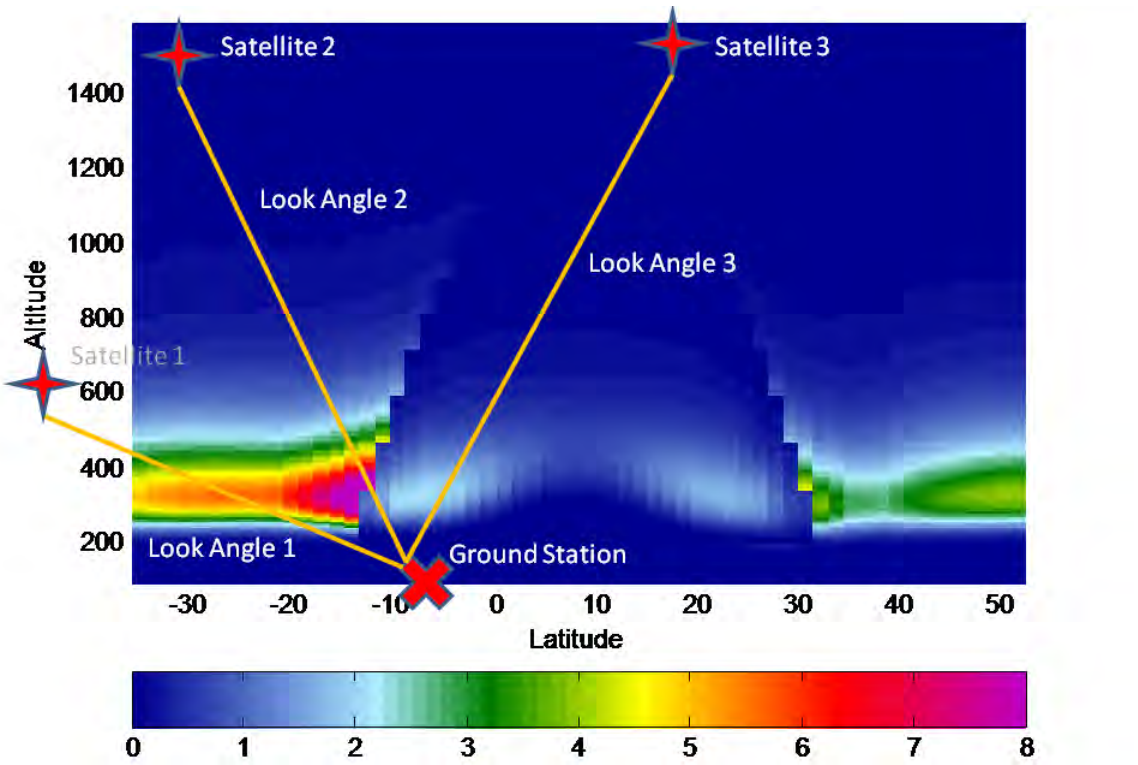

Figure 14. Selected look angles through a plasma bubble as viewed in the modified IFM electron density grid. Look angle 1 does not pass through the bubble, look angle 2 partially passes through the bubble, and look angle 3 passes through the entire bubble.

be rejected by the Kalman filter. Look angle 2 produces the measurements of the bubble that are assimilated by the model and affected by the depletion magnitude. Look angle 3 travels through most of the bubble and its TEC values are reduced beyond a depletion factor of 5 resulting in a rejection of the measurement by the Kalman filter for all three depletion factors.

Samples of elevation angles and slant TECs are given in Table 2 for conditions where there were depletion factors of 10, 100, and 1000, as well as the bubble absent case. The three elevation angles are representative of the look angles in Figure 14. For the look angle 1 case of 17 degrees the slant TEC value is unaffected by the depletion magnitude because that look angle does not pass through the bubble. In fact, for a ground

Table 4. Slant TEC values measured from 3 selected look angles through a plasma bubble placed in the modified IFM electron density grid.

		No bubbles	10x depletion	100x depletion	1000x depletion
Elevation Angle	Look Angle #	Slant TEC	Slant TEC	Slant TEC	Slant TEC
17.23	1	46.93	46.93	46.93	46.93
43.02	2	30.66	23.13	22.48	22.41
63.55	3	21.15	3.70	1.97	1.79

station centered below a plasma bubble based at 200 km with a width of 830 km or 7.5 degrees, any elevation angle less than 25 degrees will not pass through the bubble. Next, the look angle 2 case of 43 degrees passes through part of the undisturbed ionosphere and part of the bubble and is therefore only partially affected by the bubble's presence. The slant TECs for depletion factors of 10, 100, and 1000 are reduced by factors of 1.33, 1.36, and 1.37, respectively. None of the depletion factors for look angle 2 are greater than the factor of 5 cutoff of the Kalman filter and therefore the measurement will be used in all three instances. Although the factor of 1000 depletion produces a lower slant TEC for the elevation angle than the factor of 10 depletion, it is only 2% lower and consequently cannot have a large affect on GAIM-GM's output. The effect of this small difference in look angle 2 cases can be seen in panels (d) and (e) of Figure 13. Lastly, the high elevation angle of 63 degrees has depletion factors of 5.71, 10.74, and 11.82, all of which are above the factor of 5 threshold of the Kalman filter. None of the observations for the high elevation angle are assimilated by the filter and therefore have no affect on the model output for any depletion magnitude.

Small differences that are present in panels (d) and (e) of Figure 13 can be found in regions within 5 degrees of ground station locations. The differences are not found directly over the ground stations because these measurements would have had large elevation angles like look angle case 3 and been removed by the Kalman filter for all three depletion cases. Instead, the largest differences are found away from the ground station location due to look angle 2 cases and corresponding ionospheric pierce points that are removed from the ground station. Since the magnitude of the plasma bubble depletion has little effect on the output of GAIM-GM, a factor of 10 depletion was used for the remaining test cases. Next, geophysical conditions will be varied to study the effect on GAIM-GM output with bubbles present.

4.3 Geophysical Conditions Analysis

The capability of GAIM-GM to model plasma bubbles is affected by the TEC values of the background ionosphere. GAIM-GM produces weaker perturbation fields in the presence of lower background TEC values. Low TEC values of 1-2 TECU are commonly found during solar minimum nights, particularly during the solstices, diminishing the capability of GAIM-GM to add perturbations to the background state. Two geophysical conditions of relatively higher and lower background TEC values were evaluated, resulting in seasonal and solar cycle comparisons.

4.3.1 Equinox and Solstice Comparison

The results of the spring equinox and winter solstice conditions for 00, 03, and 06 UT are presented in Figure 15. Both scenarios included four plasma bubbles with factor of 10 density depletions placed in sequence over South America. Although the F10.7

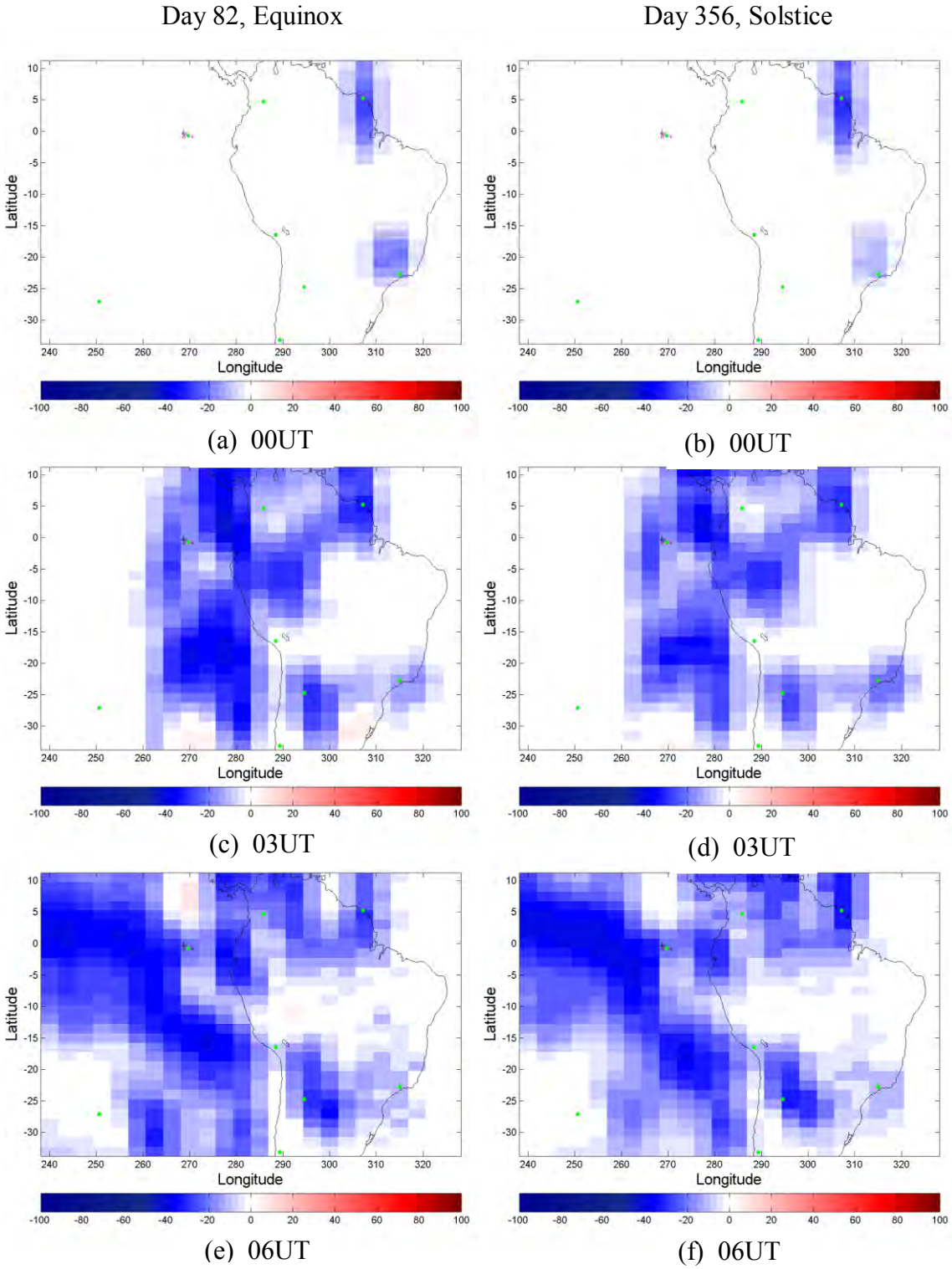

Figure 15. Comparison of percent difference maps from equinox and solstice.

value was 113 SFUs for both cases, the background TEC values of the equinox run were higher by 5-10 TECUs than the solstice run because of different solar zenith angles and seasonal differences in the background neutral densities. The result of this difference in background TEC values was that the GAIM-GM output during equinox showed stronger depletions than during the solstice. In general, GAIM-GM output generates a 10% greater depletion with the higher background levels during equinox. The regions covered by the depletions are similar because identical ground station to satellite look angles were used for both cases. With bubble absent TEC values over South America differing by as much as 25% from equinox to solstice, GAIM-GM produces up to a 10% stronger depletion in the region. Peak skill scores for the equinox case are 0.39 while for the solstice case the best scores are 0.34 for the same time period. The skill scores verify that GAIM-GM has a better performance while ingesting plasma bubble observations when the background TEC values are higher.

4.3.2 Solar Minimum and Maximum Comparison

The next test was to run GAIM-GM with plasma bubbles present during both solar minimum and solar maximum conditions. Snap shots of the output taken at 00, 03, and 06 UT are shown in Figure 16. The solar maximum graphs have larger depletions than the solar minimum case for all time steps and the percent differences are generally twice as large. At the first time step, panels (a) and (b), the largest percent difference for solar minimum is -10% while for solar minimum is it -25%. The perturbation fields move sun synchronously, become superimposed, and sum west of the bubble locations. By the 06UT panels, the largest percent differences for solar minimum and maximum are -36% and -54%, respectively. The solar maximum case has larger depletions in all areas

Solar Minimum, F10.7 = 70 Solar Maximum, F10.7 = 210

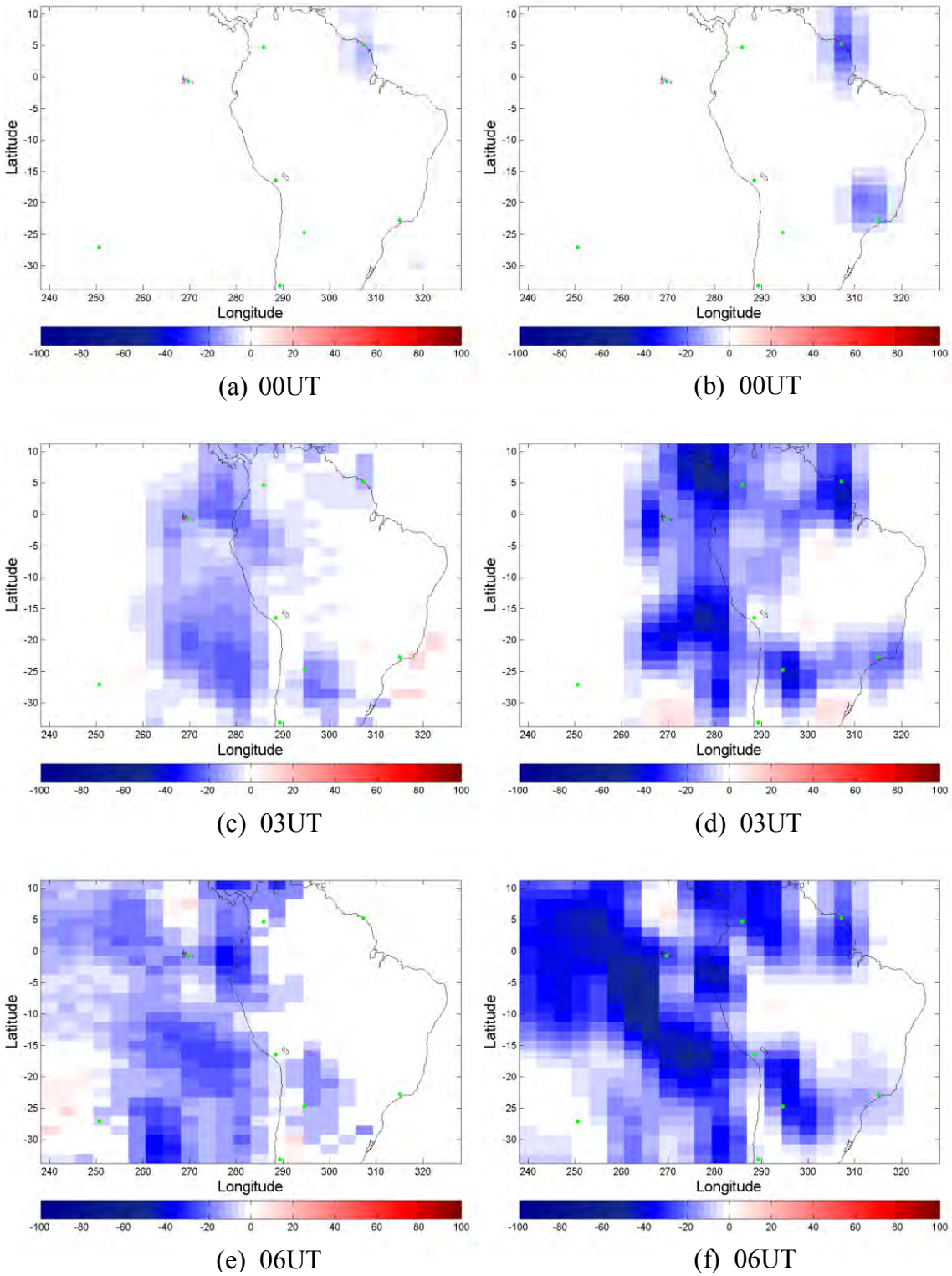

(a) 00UT (b) 00UT

(c) 03UT (d) 03UT

(e) 06UT (f) 06UT

Figure 16. Percent difference comparison between TEC output for solar minimum and maximum.

of the South American region because the background TEC values in the nightside ionosphere are larger than during solar minimum. The background TEC values during solar maximum can be up to an order of magnitude larger in the 20 to 24LT period near the equator. Since the area of the South American region covered by the depletions is the same for both cases the only difference between the GAIM-GM outputs is the percent decrease at each grid location. The solar maximum case was closer to the ideal depletion percentage of 90% and therefore is a better solution. The skill scores verify that GAIM-GM performed better during the solar maximum case, with a peak skill score of 0.29 compared to 0.18 for the solar minimum case.

4.4 Relaxation Time Analysis

The relaxation time, or time constant, controls the length of time GAIM-GM will take to relax a perturbation back to zero. GAIM-GM uses a sun synchronous movement of the perturbation field which causes differences to translate west while relaxing the density field to the background state over time. On the percent difference maps this feature manifests itself as a field of differences propagating west.

4.4.1 Changes to the Time Constant

Lowering the time constant forces perturbations to relax to the background state over a shorter time period. Because the perturbations are propagated sun synchronously by the model, the result of reducing the time constant from 5 hours to 1 hour is to reduce the westward extent of the TEC differences, shown in Figure 17. Sun synchronous movement means that a perturbation would translate 15 degrees per hour to the west. Reducing the time constant from 5 hours to 1 hour should reduced the westward extent of

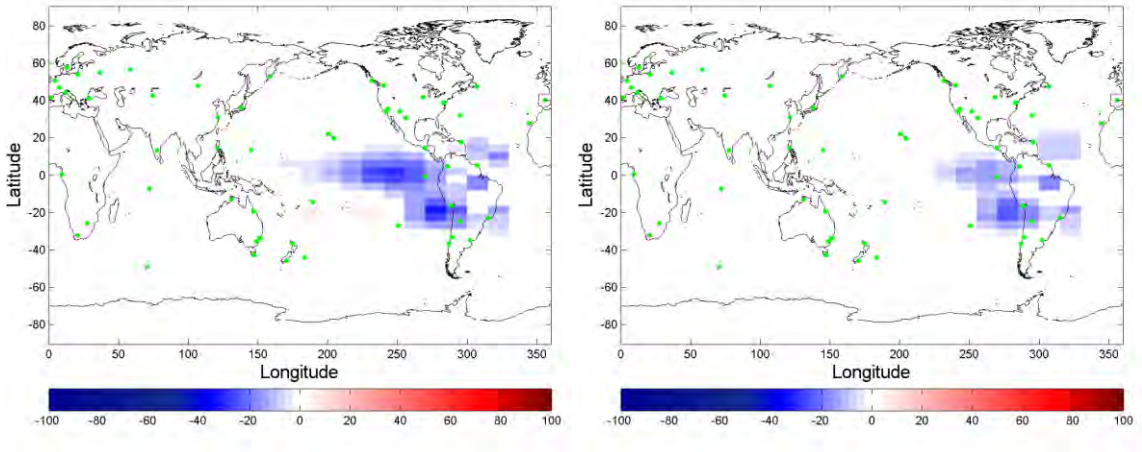

(a) Time constant = 5 hours (b) Time constant = 1 hour

Figure 17. Comparison of time constant settings for 08UT on day 82.

differences by 60 degrees. Figure 17 shows a reduction of the westward extent by 45 degrees and in general reducing the time constant reduced the westward limit of the depletions between 30 and 60 degrees.

In addition to changing the westward boundary of the perturbation field, Figure 17 also shows that the depletion had a smaller magnitude when the time constant was set to one. Lowering the time constant not only affects the distance to the west a disturbance can propagate, but also the rate at which it decays to the background state. A shorter relaxation time means the perturbation has to decay more quickly and by a larger magnitude at each time step. Four bubbles were used in this test, and each created their own perturbation fields that summed as the fields became superimposed upon one another. The result of the summed perturbation fields was to create the largest magnitude depletions west of South America. The lower time constant meant each of the four perturbations decayed faster resulting in a smaller magnitude depletion than in the default time constant case.

Another factor affecting the perturbation fields is the distribution of ground stations. When the perturbation is propagated into a region that has GPS measurements for that time step, the presence of measurements from the ground station causes the perturbation field to quickly relax. The sun synchronous extent of any perturbation field is therefore shaped by the distribution of ground stations to the west of the initial perturbation.

While a smaller spatial extent is affected by the perturbation field when a lower time constant is used, the skills scores are actually better for the higher time constant. Figure 18 shows the skill scores for regional runs of GAIM-GM with time constants set to five and one hour. The higher skill scores with the time constant set to five hours indicate that the output was closer to the ideal observation set, the IFM with bubbles present, than the lower time constant case. The reason for this result is that while the smaller disturbed area, resulting from the time constant being set to one hour, initially appears better, it is actually the larger magnitude depletions present off the west coast of South America in the time constant set to five hour case that come closer to the actual bubble observations. There is a balance between the spatial extent and magnitude of the depletion in the GAIM-GM TEC output. Lowering the time constant improves the spatial boundaries but degrades the reproduction of depletion magnitude, yielding a net worse result.

4.4.2 Sun Synchronous Bubble Movement

Since GAIM-GM moves perturbations sun synchronously the next test case was to allow the bubble to move in this manner. Although this condition is physically unrealistic, it provides an interesting result by aligning bubble movement with the sun

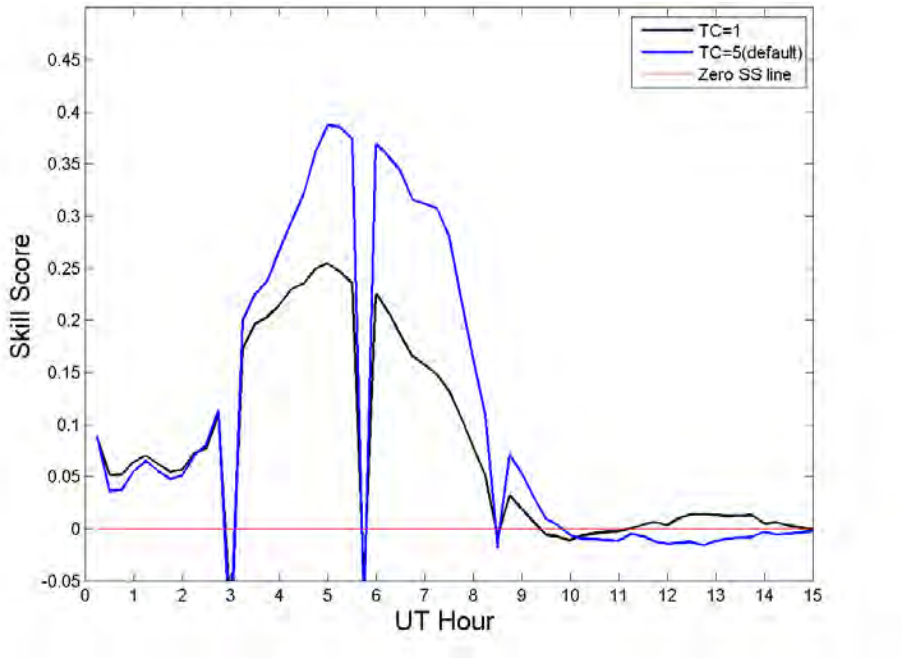

Figure 18. Skill score comparison of varying the time constant in GAIM-GM regional output for day 82.

synchronous assumption within the Kalman filter. One bubble was created over Brazil and allowed to move sun synchronously 15 degrees per hour to the west. The result of this run is presented in Figure 19 as a series of percent difference graphs between the sun synchronous case and a run of GAIM-GM with plasma bubbles absent. Panels (a) through (e) are snapshots of the GAIM-GM output at one hour increments from 00-04 UT. The bubble first appears at 00 UT and the area and magnitude of the depletion in the GAIM-GM output is similar to the 00 UT frame from previous comparisons. As time progresses in panels (b) through (e) the perturbation field moves to the west at the same rate as the bubble. The measurements GAIM-GM is receiving through the GPS inputs are matching the location of the perturbation field. The perturbation field reinforces the measurements at each time step resulting in the model successfully tracking the location of the bubble through 04 UT. The width of the bubble is approximately 11.25 degrees,

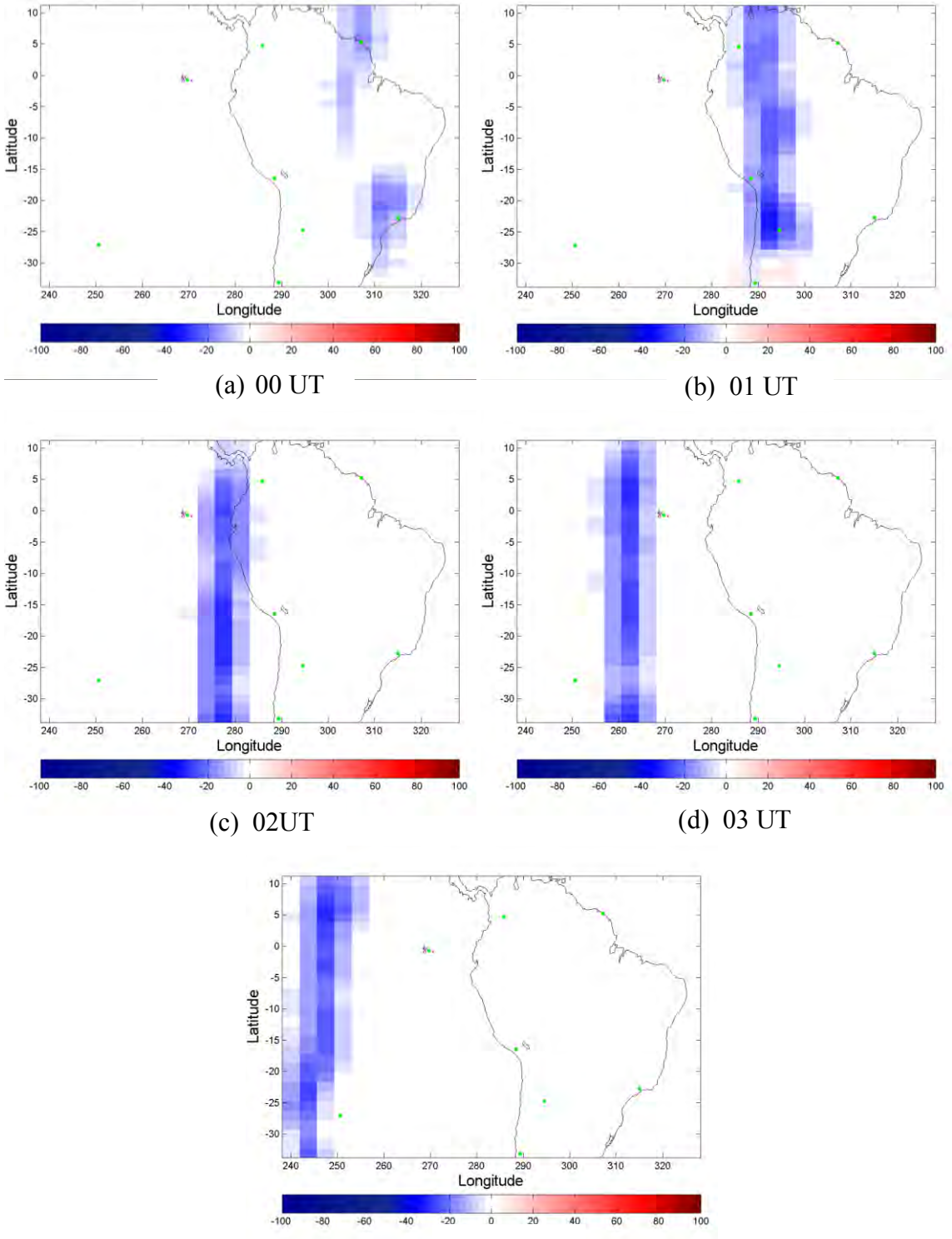

Figure 19. Percent difference maps for GAIM-GM regional output on day 82 with sun synchronous bubble measurements as inputs to the model.

about one and a half times larger than the 7.5 degree bubble that the observations were created from. The depletion magnitude is underrepresented by GAIM-GM, with a maximum depletion of 35% being significantly less than the 90% depletion that was input into the GPS measurements.

4.4.3 Super-Rotating Bubble Movement

Plasma bubble super-rotation has been observed and was tested by moving the bubbles to the east at 230 m/s, or 7.5 degrees per hour, after their formation at 20LT. The results are displayed in Figure 20 as percent difference maps. As expected from the sun synchronous assumption in the Kalman filter, the model was unable to move the perturbation fields in the correct direction towards the east and instead moved the depletions sun synchronously to the west. The perturbations fields were relaxed when bubble absent measurements over the Galapagos and Easter Islands were encountered, but extended farther west in regions that ground stations were not present. At no point was the model able to move the perturbation field into the Atlantic east of the ground station locations. Figure 7 showed the movement of the bubbles in the IFM grid.

4.5 Station Density Analysis

GAIM-GM output with the AFWA station list is compared to output with an ideal, regional grid of GPS ground stations in Figure 21. The ideal grid of ground stations provides a dense network of GPS measurements to the Kalman filter from which GAIM-GM is able to reproduce four distinct bubbles. The density depletions are centered at the correct longitudes to match the bubble input placement but the depletion

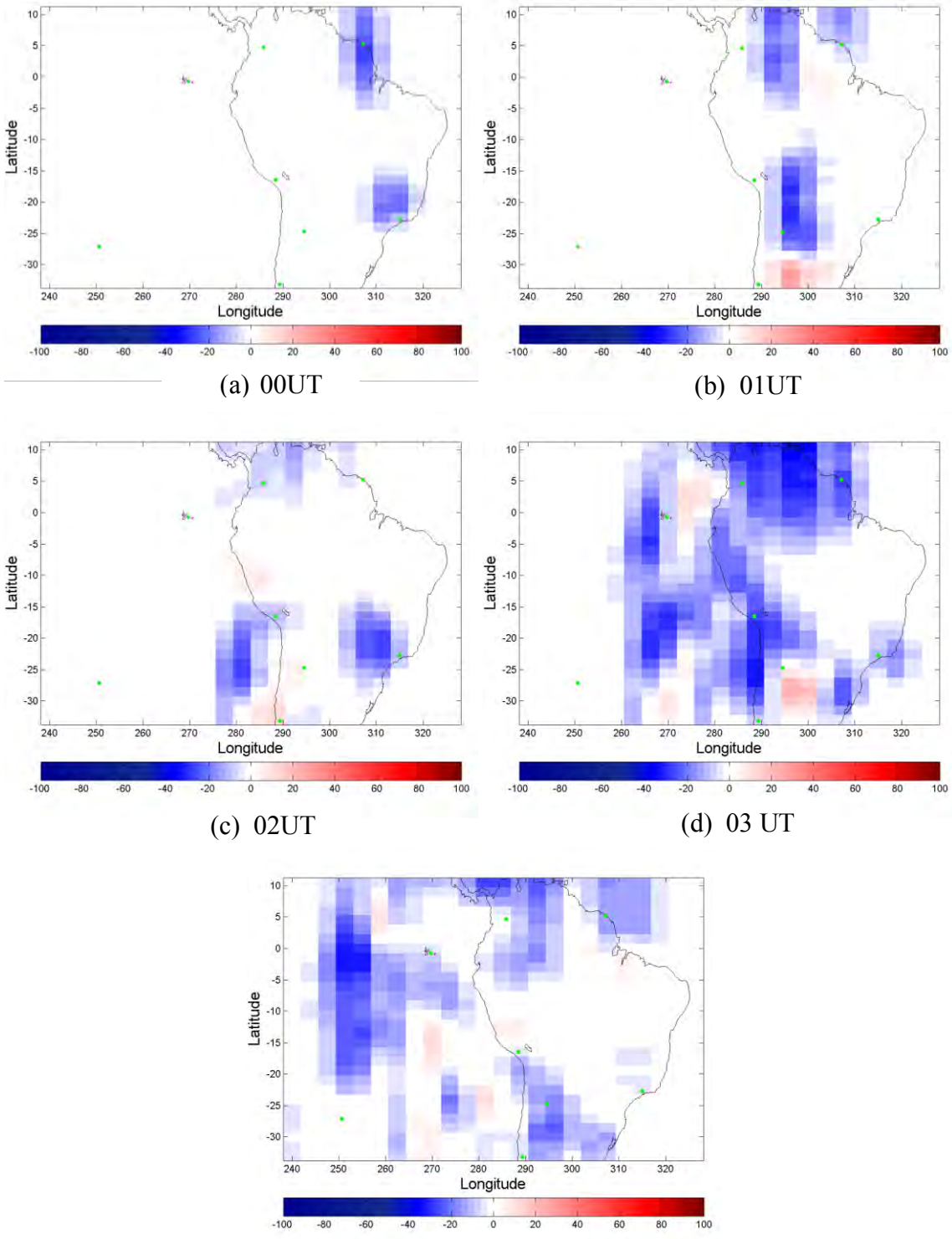

Figure 20. Percent difference maps for GAIM-GM regional output on day 82 with super-rotating bubble measurements as inputs to the model.

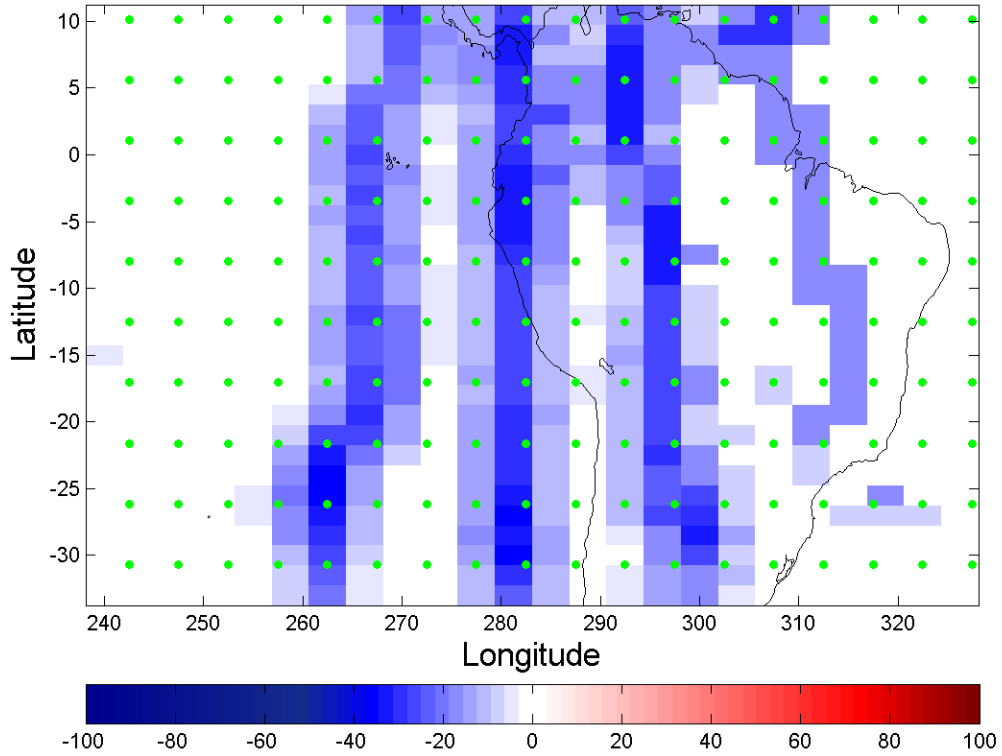

Figure 21. Percent difference map of 4 corotating plasma bubbles in an ideal regional grid for day 82.

magnitudes are below the bubble measurements. Depletion magnitudes in the GAIM-GM output were 35-40%, significantly less than the 90% depletion used in the input files.

The output with the ideal grid supports results from the time constant and geophysical conditions tests. First, GAIM-GM is able to create individual bubbles because the ideal grid density is great enough to place a line of ground stations between each bubble. The perturbation field created from the measurements at each bubble is propagated sun synchronously, but as discussed above is translated to a point with measurements from a new ground station. The measurements with bubbles absent from the ground station to the west are weighted more heavily in the Kalman filter and the perturbation field is relaxed to zero. Second, the ideal grid output has lower depletion

percent differences in the eastern bubble as compared to the western bubble. The eastern bubble lies in an area of lower background TEC values than the western bubble and supports the earlier data that GAIM-GM more reliably recreates bubble observations in higher TEC environments.

V. Discussion

The results of the plasma bubble output analyses are discussed in this chapter, including their computational and operational uses and applications. Additionally, topics for further research will be suggested and a brief summary will follow.

5.1 GAIM-GM Output Analysis

GAIM-GM is limited in its ability to model plasma bubbles because of several parameters within the Kalman filter. First, the lower bound the filter places on acceptable observed TEC values means that the highest magnitude depletion measurements will be rejected and not used within the GAIM-GM calculation. GPS measurements below this threshold are discarded by the filter because they are too far below the background model state. While it is important to protect against erroneous data, in this case the outlier data represents a real physical feature of the ionosphere. Because the filter removes observations below a factor of 5 depletion from the background state, GAIM-GM cannot depict the full magnitude of plasma bubbles with depletion factors of 5 and greater.

The next limiting factor within the Kalman filter is the assumption that perturbations move sun synchronously. Since plasma bubbles have been observed to corotate with the Earth and even super-rotate this assumption is not valid for this particular kind of perturbation. The result of the sun synchronous assumption is to incorrectly move the perturbation field to the west at a rate of 15 degrees per hour. Because the default time constant within the model is 5 hours this can result in the perturbation field extending more than 75 degrees to the west in the absence of GPS measurements. The perturbation field is erroneously changing the output TEC values

west of the actual plasma bubble location. In this study TEC changes were documented up to 100 degrees to the west for a period of up to 5 hours after the plasma bubble. This study evaluated the prospect of lowering the time constant, which was shown to limit the sun synchronous movement of the perturbation field, however the effect of this change on other features of the ionosphere was not accounted for.

Operationally, GAIM-GM's inability to capture the full magnitude of bubble depletions and the false depletion area to the west of the bubble location can lead to incorrect specifications and forecasts of the ionosphere. The electron density constructed by GAIM-GM will be incorrect in these areas leading to errors in the TEC and height and density of the F2 layer peak. The incorrect specifications and forecasts will lead to incorrect range and frequency specifications for HF radio communication.

Coupled to any perturbation field discussion is the dependence of GAIM-GM on the number of GPS ground stations available. In the absence of new observations the perturbation field is imposed upon the background state. In the presence of new observations the perturbation field is changed according to the relative weights of the new observations. This result explains the station density analysis where distinct bubbles were modeled in the ideal regional grid. Although the AFWA station list of 59 stations may seem small there aren't that many more equatorial ground stations currently in operation that could be added. The equatorial regions of the Earth are mostly ocean and low population density land, limiting the opportunity for a dense network of GPS ground stations such as is the case of the continental United States and Europe. Incorporating additional satellite data, observing the ionosphere near the dusk sector, and using GPS data from ships, can help to circumvent some of these problems.

The resolution of GAIM-GM is also a limiting factor because of the small scale of plasma bubbles. The 7.5 degree longitudinal width of the bubbles used in this study is reasonable, but extremely large for a bubble and was used because it fit well with IFM resolution while still being realistic. The 15 degree longitudinal global resolution of GAIM-GM means that individual bubbles cannot be resolved. Additionally, any observations of plasma bubble depletions will be averaged and smoothed with data from a large region, further reducing the magnitude of the depletion that GAIM-GM can model.

GAIM-GM TEC output does not provide sufficient contrast for the forecaster to locate plasma bubbles. Factor of 10 bubble depletions are only 1-2 TECU differences from the background state in the nightside ionosphere which would be difficult to find with a perfect replication of the bubble. The small difference coupled with the diffuse bubble output from GAIM-GM makes it impractical to find bubbles in the TEC output from GAIM-GM. Rather, the only way to know GAIM-GM has added a perturbation field is to use a difference map such as the ones in this study. This would require two simultaneous runs of GAIM-GM to compare and a priori knowledge of which GPS data files contained bubble observations. Even after creating difference maps the result would not be much more useful because of the limitations involving the Kalman filter discussed above.

5.2 Further Study

Next, options for further study are suggested that would further test the capabilities of GAIM-GM to model plasma bubbles.

5.2.1 Additional Data Sources

The present study only incorporated one of the several types of data GAIM-GM is capable of ingesting. Satellite occultations could be used as an additional data source for the model rather than exclusively GPS slant TEC measurements. The advantage of satellite occultations is that they can occur in any geographic location and are not tied to ground station placement like GPS measurements. Occultation measurements would have a more uniform distribution than GPS ground stations and include readings over the oceans where GPS is lacking. Additionally, incorporating GPS data from ships would increase the density of GPS measurements. Many routine shipping lanes cross equatorial regions and could potentially provide a wealth of additional information. Since real time measurements outweigh perturbation fields within the Kalman filter the presence of a more uniform grid and data over the oceans should limit the sun synchronous movement of plasma bubble perturbation field yielding a better result than GPS ground stations alone.

5.2.2 Effect of Kalman Filter Modifications

One finding of the present paper was that lowering the time constant produced a spatially improved GAIM-GM output with plasma bubbles because the perturbation fields were relaxed to background values faster. Although this result is true for bubbles it remains unknown how this change affects other features of the ionosphere. Before the time constant can be lowered in the operational model the effects of this change must be investigated to understand the changes in other regions of the ionosphere that the change will invoke.

In addition, removing the sun synchronous movement of perturbation fields should result in a better plasma bubble output from GAIM-GM. A future study to investigate this alternative, as well as its effects on other features of the ionosphere could be undertaken.

5.3 Conclusion

Overall, GAIM-GM is not capable of modeling equatorial plasma bubbles. The model does not include the physics necessary to account for bubbles and the structure of the Kalman filter results in an inaccurate recreation of the local ionosphere. Although the model is able to lower the TEC values in the region near the bubble, the area of that depletion is too large and the magnitude of the depleted values is too small. Moreover, the sun synchronous movement of perturbations by the Kalman filter propagates depleted values into regions where bubbles are not present.

The research presented in this paper is important to both the model developers and the Air Force. By understanding the limitations of the data assimilation scheme, ionospheric model developers will be able to create improved products in the future. Additionally, the Air Force can use this research to understand how the presence of plasma bubbles will affect the output of its primary ionospheric model. Knowledge of plasma bubble effects on GAIM-GM output will enable forecasters to improve forecasts and tailor products to customer needs. Decision makers will have a clearer picture of the capabilities and limitations of GAIM-GM leading to a greater probability of mission success.

Bibliography

Burke, W., C. Huang, L. Gentile, C. E. Valladares, and S. Y. Su (2004), Longitudinal Variability of Equatorial Plasma Bubbles Observed by DMSP and ROCSAT-1, *Journal of Geophysical Research, 109*(A12301).

Comberiate, J., and L. Paxton (2010), Global Ultraviolet Imager equatorial plasma bubble imaging and climatology, 2002-2007, *JOURNAL OF GEOPHYSICAL RESEARCH-SPACE PHYSICS, 115*.

Howe, B. M., and K. Runciman (1998), Tomography of the ionosphere: Four-dimensional simulations, *Radio Sci., 33*(1), 109.

Li, G., B. Ning, L. Liu, W. Wan, and J. Y. Liu (2009), Effect of Magnetic Activity on Plasma Bubbles Over Equatorial and Low-latitude Regions in East Asia, *Annales Geophysicae, 27*, 303-312.

Mannucci, A. J., B. D. Wilson, D. N. Yuan, C. H. Ho, U. J. Lindqwister, and T. F. Runge (1998), A global mapping technique for GPS-derived ionospheric total electron content measurements, *Radio Sci., 33*(3), 565-582.

Nava, O. A. *Analysis of Plasma Bubble Signatures in the Ionosphere*. MS thesis, AFIT/GAP/ENP/11-M06. School of Engineering and Management, Air Force Institute of Technology (AU), Wright-Patterson AFB OH, March 2011.

Portillo, A., M. Herraiz, S. M. Radicella, and L. Ciraolo (2008), Equatorial plasma bubbles studied using African slant total electron content observations, *Journal of Atmospheric & Solar-Terrestrial Physics, 70*(6), 907-917, doi: 10.1016/j.jastp.2007.05.019.

Sahai, Y., P. R. Fagundes, and J. A. Bittencourt (2000), Transequatorial F-region ionospheric plasma bubbles: solar cycle effects, *J.Atmos.Solar Terr.Phys., 62*(15), 1377-1383, doi: DOI: 10.1016/S1364-6826(00)00179-6.

Scherliess, L., R. W. Schunk, J. J. Sojka, D. C. Thompson, and L. Zhu (2006), Utah State University Global Assimilation of Ionospheric Measurements Gauss-Markov Kalman filter model of the ionosphere: Model description and validation, *Journal of Geophysical Research, 111*(A11315), 1.

Scherliess, L., R. W. Schunk, J. J. Sojka, and D. C. Thompson (2004), Development of a physics-based reduced state Kalman filter for the ionosphere, *Radio Sci., 39*(1), RS1S04.

Schunk, R. W., L. Scherliess, and D. C. Thompson (2011), Ionosphere Data Assimilation: Problems Associated with Missing Physics, *Aeronomy of the Earth's Atmosphere and Ionosphere, 2*, 437-442.

Schunk, R. W., and H. G. Demars (2003), Effect of Equatorial Plasma Bubbles on the Thermosphere, *Journal of Geophysical Research, 108*(a6), 1245.

Schunk, R., and A. Nagy (2009), *Ionospheres: Physics, Plasmas, and Chemistry*, 2nd ed., Cambridge University Press, New York.

Schunk, R. W., et al (2004), Global Assimilation of Ionospheric Measurements (GAIM), *39*(1), doi: 10.1029/2002RS002794.

Sinha, H. S. S., and S. Raizada (2000), Some New Features of Ionospheric Plasma Depletions over the Indian Zone Using All Sky Optical Imaging, *Earth, Planets, and Space, 52*(8), 52.

Sojka, J. J., D. C. Thompson, L. Scherliess, R. W. Schunk, and T. J. Harris (2007), Assessing models for ionospheric weather specifications over Australia during the 2004 Climate and Weather of the Sun-Earth-System (CAWSES) campaign, *Journal of Geophysical Research, 112*(A09306).

Thompson, D. C., L. Scherliess, J. J. Sojka, and R. W. Schunk (2006), The Utah State University Gauss–Markov Kalman filter of the ionosphere: The effect of slant TEC and electron density profile data on model fidelity, *J.Atmos.Solar Terr.Phys., 68*(9), 947-958, doi: DOI: 10.1016/j.jastp.2005.10.011.

Thompson, D. C., L. Scherliess, J. J. Sojka, and R. W. Schunk (2009), Plasmasphere and upper ionosphere contributions and corrections during the assimilation of GPS slant TEC, *Radio Sci., 44*, RS0A02.

Vita

Captain Kenneth R. Fenton Jr. graduated from the Marine Academy of Science and Technology on Sandy Hook, New Jersey in 2002. He entered undergraduate studies at the United States Air Force Academy in Colorado Springs, Colorado where, in May 2006, he graduated with a Bachelor of Science degree in Meteorology and received his commission as a Second Lieutenant in the United States Air Force.

For his first assignment, Captain Fenton was assigned to Hickam Air Force Base in Honolulu, Hawaii where he served as a lead meteorologist and flight commander for the 17th Operational Weather Squadron. After three years in Hawaii, he was selected to enter the Graduate School of Engineering and Management at the Air Force Institute of Technology at Wright-Patterson Air Force Base, Ohio in October 2009. Upon graduation, he will be assigned to the 16th Weather Squadron at Offutt Air Force Base.

REPORT DOCUMENTATION PAGE

Form Approved
OMB No. 074-0188

PLEASE DO NOT RETURN YOUR FORM TO THE ABOVE ADDRESS.

1. REPORT DATE *(DD-MM-YYYY)*	2. REPORT TYPE	3. DATES COVERED *(From – To)*
09-15-2011	Master's Thesis	June 2010 – September 2011

TITLE AND SUBTITLE

Assessment of the Effects of Plasma Bubbles on GAIM-GM

5a. CONTRACT NUMBER

5b. GRANT NUMBER

5c. PROGRAM ELEMENT NUMBER

6. AUTHOR(S)

Fenton, Kenneth R., Captain, USAF

5d. PROJECT NUMBER
If funded, enter ENR #

5e. TASK NUMBER

5f. WORK UNIT NUMBER

7. PERFORMING ORGANIZATION NAMES(S) AND ADDRESS(S)
Air Force Institute of Technology
Graduate School of Engineering and Management (AFIT/ENY)
2950 Hobson Way, Building 640
WPAFB OH 45433-8865

8. PERFORMING ORGANIZATION REPORT NUMBER

AFIT/GAP/ENP/11-S02

9. SPONSORING/MONITORING AGENCY NAME(S) AND ADDRESS(ES)
Air Force Weather Agency
Attn: Capt Janelle Jenniges
101 Nelson Drive
OFFUTT AFB NE 68113-0690
CMCL: 402-294-0690
EMAIL:2SYOSDOR@offutt.af.mil

10. SPONSOR/MONITOR'S ACRONYM(S)
AFWA

11. SPONSOR/MONITOR'S REPORT NUMBER(S)

12. DISTRIBUTION/AVAILABILITY STATEMENT
APPROVED FOR PUBLIC RELEASE; DISTRIBUTION UNLIMITED.

13. SUPPLEMENTARY NOTES

14. ABSTRACT
Plasma bubbles are regions of depleted plasma density generated in the post-sunset equatorial region of the ionosphere. Bubbles significantly affect total electron count (TEC) and consequently alter communication and navigation capabilities. Here, the Global Assimilation of Ionospheric Measurements Gauss-Markov (GAIM-GM) model is studied in order to assess its capability to accurately model equatorial plasma bubbles. GAIM-GM uses the Ionospheric Forecast Model (IFM) as a background state modified through the application of a Kalman Filter to incorporate ionospheric observations such as Global Positioning System (GPS) total electron content (TEC) values. GPS TEC values representative of plasma bubble conditions are modeled and input into GAIM-GM along with a background IFM state and compared with GAIM-GM model runs with plasma bubbles absent. The model resolution, bubble depletion factor, filter time constant, and geophysical conditions are varied to assess model response. GAIM-GM is unable to reliably model plasma bubble magnitude and spatial extent due to several characteristics of the model and filter. The resolution of GAIM-GM, in both regional and global modes, is insufficient to capture the small scale of bubbles. Additionally, the sun synchronous movement of perturbations and lower bound of the Kalman filter affect the location and magnitude of depletion regions in the model.

15. SUBJECT TERMS
Plasma Bubble, GAIM-GM, Space Weather

16. SECURITY CLASSIFICATION OF:			17. LIMITATION OF ABSTRACT	18. NUMBER OF PAGES	19a. NAME OF RESPONSIBLE PERSON
a. REPORT	b. ABSTRACT	c. THIS PAGE			Dr. William F. Bailey, AFIT/ENP
U	U	U	UU	74	19b. TELEPHONE NUMBER *(Include area code)* (937) 255-3636, ext 4501 william.bailey@afit.edu

Standard Form 298 (Rev. 8-98)
Prescribed by ANSI Std. Z39-18